# STUDIES ON NANOPLASTICS FOR THE PREPARATION OF REFERENCE MATERIALS

Inaugural dissertation

to obtain the academic degree

DOCTOR RERUM NATURALIUM (DR. RER. NAT.)

in the scientific discipline "Colloidal and Polymer Chemistry"

submitted to the

Faculty of Science


by

JANA HILDEBRANDT

Research performed at
Bundesanstalt für Materialforschung und -prüfung (BAM)

Disputation: 06/11/2023

Unless otherwise indicated, this work is licensed under a Creative Commons License Attribution 4.0 International.
This does not apply to quoted content and works based on other permissions.
To view a copy of this licence visit:
https://creativecommons.org/licenses/by/4.0

The research presented in this dissertation was carried out under the supervision of Andreas F. Thunemann between October 2019 and March 2023 at the Division Synthesis and Scattering of nanostructured Materials of the Bundesanstalt fur Materialforschung und -prufung (BAM).

1st Reviewer: Prof Dr Andreas Taubert
University of Potsdam
2nd Reviewer: Dr habil. Andreas F. Thunemann
Bundesanstalt fur Materialforschung und -prufung (BAM)
3rd Reviewer: Prof Dr Michael Gradzielski
Technische Universitat Berlin

Date of Disputation: 06/11/2023

Published online on the
Publication Server of the University of Potsdam:
https://doi.org/10.25932/publishup-61710
https://nbn-resolving.org/urn:nbn:de:kobv:517-opus4-617102

Dedicated to my family.

# ABSTRACT

The present work focuses on the preparation and characterisation of various nanoplastic reference material candidates. Nanoplastics are plastic particles in a size range of $1 - 1000$ nm. The term has emerged in recent years as a distinction from the larger microplastic ($1 - 1000$ µm). Since the properties of the two plastic particles differ significantly due to their size, it is important to have nanoplastic reference material. This was produced for the polymer types polypropylene (PP) and polyethylene (PE) as well as poly(lactic acid) (PLA).

A top-down method was used to produce the nanoplastic for the polyolefins PP and PE (Section 3.1). The material was crushed in acetone using an Ultra-Turrax disperser and then transferred to water. This process produces reproducible results when repeated, making it suitable for the production of a reference material candidate. The resulting dispersions were investigated using dynamic and electrophoretic light scattering. The dispersion of PP particles gave a mean hydrodynamic diameter $D_\mathrm{h} = 180.5 \pm 5.8$ nm with a PDI $= 0.08 \pm 0.02$ and a zeta potential $\zeta = -43.0 \pm 2.0$ mV. For the PE particles, a diameter $D_\mathrm{h} = 344.5 \pm 34.6$ nm, with a PDI $= 0.39 \pm 0.04$ and a zeta potential of $\zeta = -40.0 \pm 4.2$ mV was measured. This means that both dispersions are nanoplastics, as the particles are $< 1000$ nm. Furthermore, the starting material of these polyolefin particles was mixed with a gold salt and thereby the nanoplastic production was repeated in order to obtain nanoplastic particles doped with gold, which should simplify the detection of the particles.

In addition to the top-down approach, a bottom-up method was chosen for the PLA (Section 3.2). Here, the polymer was first dissolved in THF and stabilised with a surfactant. Then water was added and THF evaporated, leaving an aqueous PLA dispersion. This experiment was also investigated using dynamic light scattering and, when repeated, yielded reproducible results, i. e. an average hydrodynamic diameter of $D_\mathrm{h} = 89.2 \pm 3.0$ nm. Since the mass concentration of PLA in the dispersion is known due to the production method, a Python notebook was tested for these samples to calculate the number and mass concentration of nano(plastic) particles using the MALS results. Similar to the plastic produced in Section 3.1, gold was also incorporated into the particle, which was achieved by adding a dispersion of gold clusters with a diameter of $D = 1.15$ nm in an ionic liquid (IL) in the production process. Here, the preparation of the gold clusters in the ionic liquid 1-ethyl-3-methylimidazolium dicyanamide ([Emim][DCA]) represented the first use of an IL both as a reducing agent for gold and as a solvent for the gold clusters. Two volumes of

gold cluster dispersion were added during the PLA particle synthesis. The addition of the gold clusters leads to much larger particles. The nanoPLA with 0.8% Au has a diameter of $D_h = 198.0 \pm 10.8$ nm and the nanoPLA with 4.9% Au has a diameter of $D_h = 259.1 \pm 23.7$ nm. First investigations by TEM imaging show that the nanoPLA particles form hollow spheres when gold clusters are added. However, the mechanism leading to these structures remains unclear.

# KURZZUSAMMENFASSUNG

Die vorliegende Arbeit beschäftigt sich mit der Herstellung und Charakterisierung verschiedener Nanoplastikreferenzmaterialkandidaten. Um Nanoplastik handelt es sich bei Plastikpartikeln in einem Größenbereich von $1 - 1000$ nm. Der Begriff hat sich in den letzten Jahren als Abgrenzung zu dem größeren Mikroplastik ($1 - 1000$ µm) herausgebildet. Da sich die Eigenschaften der beiden Plastikpartikel auf Grund ihrer Größe deutlich unterscheiden, ist es wichtig, Nanoplastikreferenzmaterial zur Verfügung zu stellen. Dieses wurde für die Polymertypen Polypropylen (PP) und Polyethylen (PE) sowie Polymilchsäure (PLA) hergestellt.

Dabei wurde für die Polyolefine PP und PE eine top-down Methode für die Herstellung des Nanoplastiks angewandt (Abschnitt 3.1). Dazu wurde das Material mithilfe eines Ultra-Turrax Dispergiergeräts in Aceton zerkleinert und danach in Wasser überführt. Dieser Prozess führt bei Wiederholung zu ähnlichen Ergebnissen, was ihn passend für die Herstellung eines Referenzmaterialkandidaten macht. Die entstandenen Dispersionen wurden mit der dynamischen und elektrophoretischen Lichtstreuung untersucht. Die Dispersion von PP-Partikeln ergab einen mittleren hydrodynamischen Durchmesser $D_\mathrm{h} = 180.5 \pm 5.8$ nm mit einem PDI $= 0.08 \pm 0.02$ und einem Zetapotential $\zeta = -43.0 \pm 2.0$ mV. Bei den PE-Partikeln wurde ein Durchmesser $D_\mathrm{h} = 344.5 \pm 34.6$ nm, mit einem PDI $= 0.39 \pm 0.04$ und einem Zetapotential von $\zeta = -40.0 \pm 4.2$ mV gemessen. Damit handelt es sich bei beiden Dispersionen um Nanoplastik, da die Partikel $< 1000$ nm sind. Des Weiteren wurde das Ausgangsmaterial dieser Polyolefinpartikel mit einem Goldsalz versetzt und damit die Nanoplastikherstellung wiederholt, um mit Gold dotierte Nanoplastikpartikel zu erhalten, die die Detektion der Partikel vereinfachen sollen.

Neben dem Top-down Ansatz wurde für das PLA eine Bottom-up Methode gewählt (Abschnitt 3.2). Hierbei wurde das Polymer in THF zunächst gelöst und mit einem Tensid stabilisiert. Dann wurde Wasser hinzugegeben und das THF verdampft, sodass eine wässrige PLA-Dispersion übrig blieb. Auch dieses Experiment wurde mithilfe der dynamischen Lichtstreuung untersucht und führte bei Wiederholung zu reproduzierbaren Ergebnissen von einem mittleren hydrodynamischen Durchmesser von $D_\mathrm{h} = 89.2 \pm 3.0$ nm. Da durch die Herstellungsweise die Massenkonzentration von PLA in der Dispersion bekannt ist, wurde für diese Proben ein Python Notebook getestet, das die Zahlen- und Massenkonzentration von Nano(plastik)partikeln mithilfe der MALS-Ergebnisse errechnen soll. Ähnlich wie für das in

Abschnitt 3.1 hergestellte Plastik wurde auch hier Gold in den Partikel eingearbeitet, was durch die Zugabe einer Dispersion von Goldclustern mit einem Durchmesser von $D = 1.15$ nm in einer ionischen Flüssigkeit (IL) im Herstellungsprozess gelang. Dabei stellte die Herstellung der Goldcluster in der ionischen Flüssigkeit 1-Ethyl-3-methylimidazolium-dicyanamid ([Emim][DCA]) die erstmalige Verwendung einer IL sowohl als Reduktionsmittel für Gold als auch als Lösungsmittel für die Goldcluster dar. Während der Synthese der PLA-Partikel wurden zwei unterschiedliche Volumina der Goldcluster-Dispersion hinzugefügt. Die Zugabe von Goldclustern führt zu wesentlich größeren Partikeln. Das nanoPLA mit 0.8% Au hat einen Durchmesser von $D_\mathrm{h} = 198.0 \pm 10.8$ nm und das nanoPLA mit 4.9% Au hat einen Durchmesser von $D_\mathrm{h} = 259.1 \pm 23.7$ nm. Dabei zeigen erste Untersuchungen mittels TEM-Bildgebung, dass die nanoPLA-Partikel Hohlkugeln bilden, wenn Goldcluster hinzugefügt werden. Jedoch ist der Mechanismus, der zu diesen Strukturen führt, noch unklar.

CONTENTS

# 1 INTRODUCTION

Hardly any other man-made material has changed the human lifestyle as much as plastics. It all began about 100 years ago, when HERMANN STAUDINGER postulated the theory of macromolecules [1].

Research in this new field of chemistry grew steadily [2]. Another big step was the discovery of the simplified catalytic polymerization of high molecular mass polyolefins by KARL ZIEGLER and GUILIO NATTA, in the 1950s [3, 4], which was honoured with the Nobel Prize in Chemistry in 1963. The new Ziegler-Natta method made polyethylene (PE) and polypropylene (PP) production a lot cheaper and led to the increasing use of plastics in a vast field of applications. Global polymer production increased from yearly 2 million metric tons in 1950 to 381 million metric tons in 2015, which is shown in Figure 1.1. At the same time, more than half of the polymer types produced is

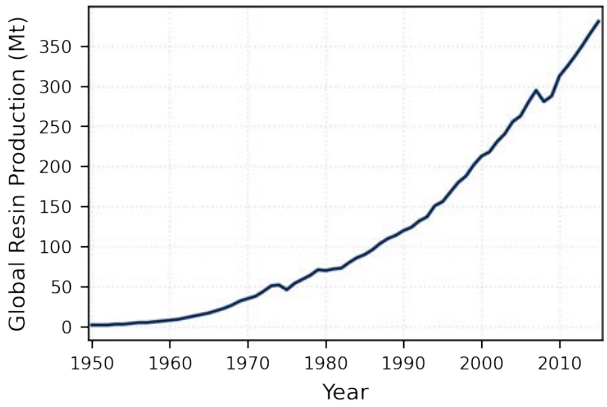


Figure 1.1: Increase of global polymer production over the years in million metric tons. Data from [5].

a polyolefin [5]. While initially, the new material class was used in more permanent applications, such as electronics, construction etc, a huge share of the plastic produced nowadays is used in the packaging sector [5]. Here, the plastics used for packaging are ca. 45% of the total plastics used globally between 2002 to 2014 [5]. Because of their chemical resistance to a broad range of chemicals, polyolefins are a popular polymer used for packaging. Most packaging is disposable and is used only once and trashed after a period of ca. 6 months [5]. All these factors result in the fact, that the ratio of trashed plastic to plastic produced annually is very high for the polyolefins PP and PE. The rates of waste generated are the highest for the different types of PE and PP, only surpassed by poly(ethylene terephthalate) (PET), which

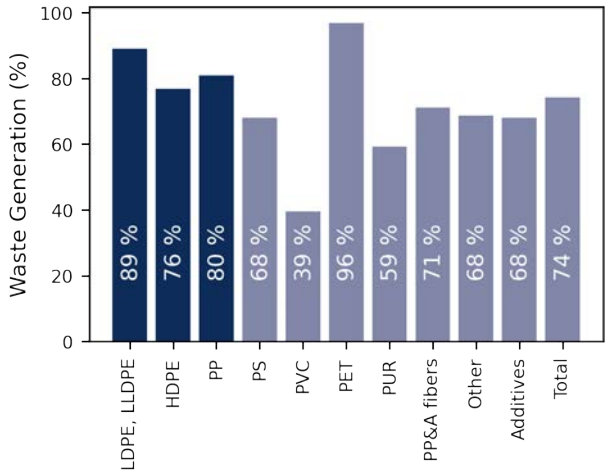


Figure 1.2: Percentages of plastic trashed of the plastic produced annually for the most common polymer types. Data from [5].

is the main material of plastic water bottles. The rates of waste generation do not necessarily pose harm to the environment if sufficient recycling is established for all types of plastics. However, this is not the case and some plastic waste is not properly disposed of. Over time, rising amounts of plastic waste ended up in the environment. Geyer et al. estimated, that 60 % of the plastic ever produced was discarded. This means, that it entered the environment through landfills or the uncontrolled disposal of plastic into nature and only a small share of the plastic ever produced was recycled (9 %) or incinerated (12 %) [5]. If plastic enters the environment, different degradation processes can occur, depending on the exact conditions. The degradation process can take place due to biological, chemical or mechanical stress. Most of the time, a combination of the three of them takes place. Then, secondary microplastics are formed. The degradation process does not stop after the formation of microplastics. The small plastic particles can degrade to even smaller particles, that are too small to be seen by the human eye. Since researchers in the field of microplastic and nanoplastic are aware that nanoplastics have significantly different effects on the environment due to their much smaller size, a distinction is made between microplastics with a diameter of $1 - 1000$ µm and nanoplastics with a diameter of $1 - 1000$ nm. The first extensive study on microplastic found in the environment was the work of R. Thompson from the University of Plymouth in 2004 [6]. In the years since then, the research in this field grew rapidly, which also led to better sample collection and detection methods, that have been defined as standards.

However, the detection of microplastics and nanoplastics from an environmental matrix only represents one field in this research topic. Toxicological tests and risk assessments are important because microplastics and especially nanoplastics are expected to interact with

human or marine organisms. Model materials are used to control the amount of plastic debris, e. g. marine organisms are exposed to in these experiments [7]. Mostly, researchers use plastic particles that were produced to serve another purpose, such as nano-sized polystyrene (PS) [8]. Via mini-emulsion polymerisation, these nanoparticles are easy to synthesise [9] and are therefore easily purchasable. However, these spherical nanoparticles do not represent the nanoplastic we are exposed to in our environment. Furthermore, they usually need surfactants to provide their colloidal stability, which can interfere with the tests [10]. Due to the lack of alternatives, they are still used, even though they do not show the same characteristics as environmentally degraded nanoplastics. Since PP and PE are very commonly used in the modern plastic industry, nanoplastic materials used for toxicological testing should contain these polyolefins. In this work, the main aim is to present a way to close this void in the field of nanoplastic research and prepare reference materials produced from the most common polymer types, that can serve as a model for environmental nanoplastic in toxicological tests and detection method validation.

# 2 THEORETICAL BACKGROUND

## 2.1 NANOPARTICLES

The term nanoparticle describes atomic or molecular compounds with at least one dimension in the size range of 1 to 100 nm [11]. The first part of the term derives from the ancient Greek word *nanos*, which means dwarf and is used as a prefix for SI unit names for values in the order of $10^{-9}$. Nanoparticles (NPs) can be composed of a wide variety of materials. In addition to metallic, inorganic, and organic particles, there are also polymer particles.

NPs have been produced for centuries even before their existence was known. Silver and gold NPs are responsible for the changing colours in dichroic glass, with the most famous example being the Roman *Lycurgus cup* [12]. NPs are also called colloids because they are usually dispersed in a liquid medium and form a colloidal suspension (*sol*).

In general, the surface of NPs is very determinant of their properties. Due to their small size, they have a huge surface atoms to core atoms ratio. The smaller the particle, the larger this ratio.This characteristic makes them very interesting for a huge variety of applications, such as catalysis, drug delivery, sensing, electronics, and cellular imaging [13–19].

The upper size limit of NPs of 100 nm was set, because many of the NPs show a certain behaviour in their optical properties for sizes below 100 nm. That is because the electronic and optical properties of NPs usually differ from those of the macroscopic material.

The quantum confinement effect leads to more discrete energy levels in very small (semi)conductive NPs and therefore to a larger band gap, the smaller the particle size is. This leads to size-dependent colours of certain nanoparticles. The majority are the so-called quantum dots (QDs), which are semiconductive nanocrystals. The adjustable photoluminescence makes QDs interesting for optoelectronic uses.

The colour of the gold and silver NPs, which are responsible for the colour of the dichroic glass, bases on the localised surface plasmon resonance in the nano-sized crystals [20]. This leads to colours of Au NPs dispersions that vary from red to purple and violet, depending on the particle size [21].

Even though, NPs show very interesting properties, they can pose harm to humans. Because of their small size, they have the potential to penetrate tissue. They are in the same size range as other biological structures such as antibodies, proteins and viruses [22]. Therefore

the potential impact on biological systems is estimated to be high and a new field of nanotoxicology research was founded. It needs to be tested whether the benefit that an application of NPs brings, also brings potential harm. Because they are usually fabricated to serve a certain application and are then released to the human environment, risk assessment studies are easier to perform beforehand. With the formation of secondary NPs in the environment after releasing certain debris to the environment, risk assessment studies are more difficult, because the right model material is in most cases not given.

### 2.1.1 *Nanoparticle Synthesis Strategies*

In general, the synthesis of NPs is distinguished between a top-down and a bottom-up method. While for the top-down method, the bulk material is crushed to fragments in the nm scale, the bottom-up strategy assembles the nanoparticle from its building blocks (atoms or molecules). There are several different strategies to achieve this. An overview is given in Table 2.1 and more details can be found in the review by Habibullah et al. [23]. The synthesis method of choice depends considerably on the NP material. While inorganic NPs are usually produced using a bottom-up approach, other NPs (especially microplastic and nanoplastic) are usually produced using a top-down approach.

Table 2.1: List of nanoparticle synthesis strategies often used. Distinguished between top-down and bottom-up methods [23].

| TOP-DOWN METHOD | BOTTOM-UP METHOD |
|---|---|
| laser ablation | electrochemical synthesis |
| sputtering | (microwave-induced) green synthesis |
| pyrolysis | chemical synthesis |
| (ball) milling | radiation-induced synthesis |
| lithography | microemulsion synthesis |

The choice of synthesis method also depends on the desired properties of the final product. In chemical syntheses, which follow a bottom-up method, it is often easy to achieve different sizes and size distributions by changing the reaction temperature and time and specifically controlling the product properties [24–26].

When it comes to plastic NPs, the method of choice is usually microemulsion [27] and miniemulsion polymerisation [9, 28]. Here, the size of the resulting NPs can be achieved directly during the polymerisation of the monomers with the amount of surfactant used [9, 29]. It makes commercial plastic nanoparticle production possible.

Unfortunately, this method is not applicable to all kinds of polymers, because the monomer needs to be emulsified.

### 2.1.2 *Colloidal Stability*

Thermodynamic stability is a central consideration when looking at nanoparticle dispersions. Mostly, these dispersions are kinetically stable. Usually, there are relatively long-range attractive forces that act on the particles and would lead to a collapse of the dispersion. There are two ways to colloidally stabilise nanoparticles and prevent aggregation. Very often surfactants are attached to the particle surface to sterically stabilise the particles and prevent the contact of two particles with a protective film, which is hard to penetrate. This method offers long-term stability for NPs. The surface molecules influence the interaction with the environment. Another possibility is electrostatic stabilisation. The electrostatic stabilisation is described by the DLVO (DERJAGUIN-LANDAU-VERWEY-OVERBEEK) theory and it combines different repulsive and attractive forces in the colloidal system. It applies to colloidal systems, where the particles have a surface charge, that is compensated by counter ions diffusely surrounding the particle surface. The surface charge and the diffusely distributed counter ions are called electrochemical double layer. There are different models that describe the electrochemical double layer at an interface. The STERN model combines the HELMHOLTZ and the GOUY-CHAPMAN model.

Negatively charged, solvated ions accumulate on the positively charged solid surface. The center of these solvated anions is called the outer Helmholtz plane. The Helmholtz model does not take into account thermal motion. After the outer Helmholtz plane, the ions are more widely distributed. The counterion (i.e. anions) predominates in contrast to the cations. At some point, the concentration of anions and cations is the same again and the diffuse double layer after the Gouy-Chapman model is finished. The Gouy-Chapman model takes into account the thermal motion but does not sufficiently consider the rigid plane at the interface. The course of the potential in the described system can be seen in Figure 2.1 on the right side. The potential of the positively charged material $\varphi_{solid}$ is constant over the full width of the solid. At the surface, it decreases linearly until the outer Helmholtz plane is reached. After the Helmholtz plane, the potential decreases exponentially over the width of the diffuse double layer, until eventually, the potential of the solution ($\varphi_{solvent}$) is reached. The potential at the end of the diffuse double layer is also called $\zeta$ potential and is a measure of the surface charge. This double layer is always present in the interface in a two-phase system with a fluid continuous phase. Because of the high surface area of colloids, the double layer is very important to determine the characteristics of a dispersion. While there are the attractive van der Waals forces, there

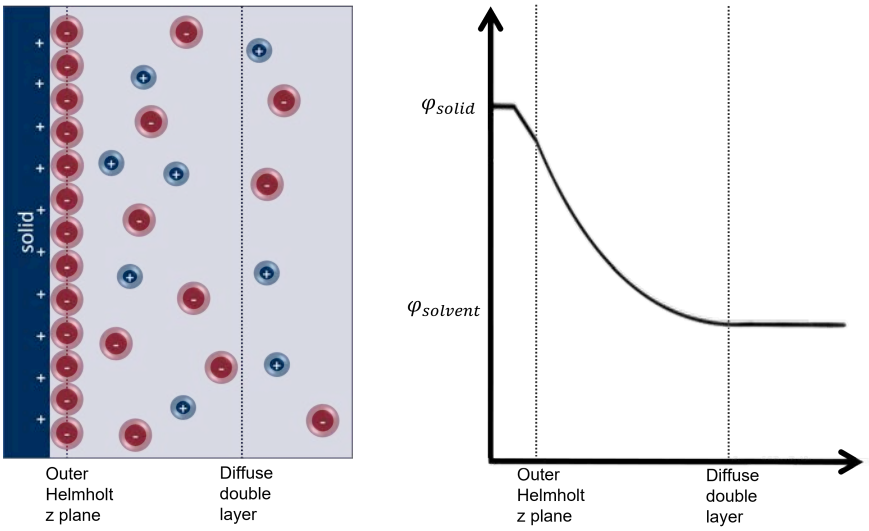


Figure 2.1: Left: Schematic structure of the electrochemical double layer at the interface of a positively charged surface in a polar solvent. Negatively charged counterions are present on the surface. The centre of this layer of counterions is also called the outer Helmholtz plane. Behind this Helmholtz plane, the counterions are less concentrated until the charges are finally balanced. Right: Graph with the potential curve along the double layer. The potential is constant in the solid and decreases with an increasing distance to the surface. Eventually, the potential of the pure solvent is reached. Figures adapted from [30].

are also the repulsive interactions coming from the double layer in a colloidal system. The potential for all interactions, therefore, is the sum of attractive and repulsive potential energies. When the double layer is thin (considerably smaller than the size of the particle), the total potential energies form a curve similar to the graph in Figure 2.2.

There is a local minimum at larger distances, where the dispersion is temporarily unstable. This is called agglomeration, which results in flocculation or sedimentation of the agglomerates. In this state, the system can be brought back into a stable state by agitation. A dispersion is usually stable when the local maximum is big enough so that it forms a barrier against the agglomeration minimum. The total balance of the potential energies is unique for every colloidal system.

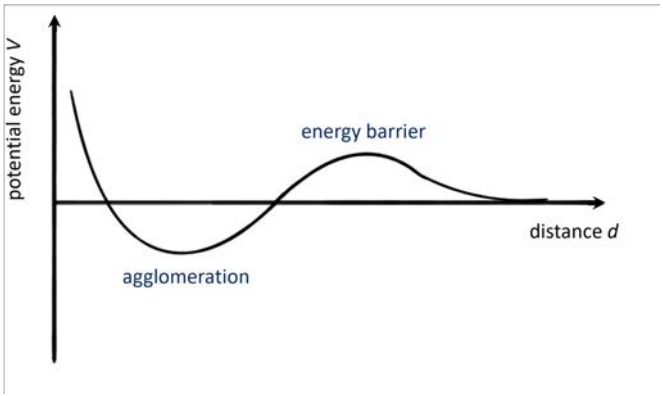


Figure 2.2: Schematic curve of the potential energies $V$ as a function of the distance $d$ of particles in a colloidal system due to the different attractive (negative $V$) and repulsive (positive $V$) forces in the system. The energy barrier (local maximum) keeps a colloidal system stable. For lower inter-particle distances a minimum is reached and the particles can agglomerate. This curve is unique for every colloidal system. Figure adapted from [30].

## 2.2 POLYMERS

In the 19$^{th}$ and the beginning of the 20$^{th}$ century, alternatives for the natural products ivory, rubber, etc. were highly sought after. The two world wars accelerated the development. This led to extensive research in finding artificial replacements. The first completely synthetic plastic was the product of the polycondensation of phenol and formaldehyde, which was called after its inventor. *Baekelite* was patented in 1907 and was only the start of fully-synthetic polymers. Its properties were suitable for several purposes. As an insulating material, it was used in electronic devices such as telephones etc. and helped to favour the electrification [2].

Firstly, the technically interesting properties of these materials were used without further knowledge of the reason for them. The possibilities for determining the structure of molecules were limited in these times. Polymers are macromolecules, that consist of one or more repeating units, called monomers. The term *polymer* is composed of the ancient Greek words *poly* and *meros* and means many parts. The term polymer covers synthetic as well as natural macromolecules (e. g. proteins and DNA). On the other hand, plastic is a type of polymer, that is completely man-made. The term *plastic* comes from the Greek word *plastikos* which means capable of being moulded and describes very well, what turns a polymer into plastic. To achieve this property, plasticisers and sometimes other additives such as dyes and stabilisers are added to most synthetic polymers. Because the polymers studied in micro- and nanoplastics research are almost exclusively processed plastic, the term plastic is used here.

Nonetheless, the benefits of these plastics made the production very interesting for a broad range of applications. The areas of application for plastic seem limitless, as there is also a suitable polymer (or combination) for most applications. Besides food packaging [31], building materials [32], adhesives [33], fabrics [34], agriculture [35] there are also several medical applications. The most popular medical used polymers are found in dental composite resins [36] but also artificial joint implants are made of polymers [37].

The versatile use of polymers in the industry led to the exponential growth of polymer production. Global polymer resin production increased from yearly 2 million metric tons in 1950 to 381 million metric tons in 2015 [5]. The global economic crises in the 1970s and late 2000s held up the growth only briefly. At the same time, more than half of the polymers produced are polyolefins.[5] Polyolefins are polymers that are manufactured by chain polymerization of alkenes, i. e. ethene, propene, but-1-ene and 2-methylprop-1-ene (isobutene). In this group of polymers, polypropylene (PP) and polyethylene (PE) are the most commonly used. Due to the different properties, PE is often distinguished between low-density (LDPE) and high-density PE (HDPE).

Polyolefins are highly used as packaging material [5]. One reason is the high chemical resistance of these materials, which leads to low interaction with the product. Furthermore, they are thermoplastics and can be easily shaped into convenient packaging forms but also do not break as easily as glass containers, etc.

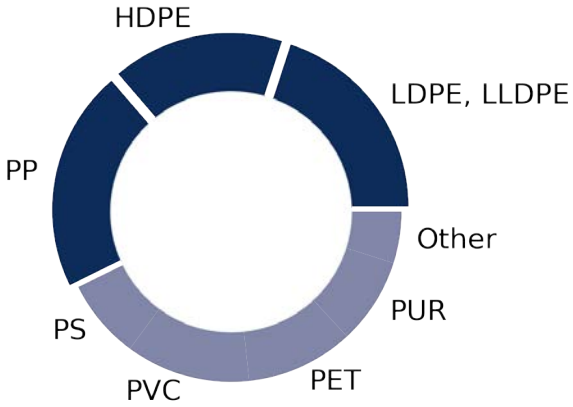


Figure 2.3: Share of different polymer types in polymer production from 2002 to 2014 [5]. PP, HDPE, LDPE, and LLDPE sum up to more than 50% of the total polymers produced.

Plastic packaging is very often trashed after a single use and has only a short-termed life. A mean life span of 6 months is assumed for plastic packaging [5]. For many years, plastic litter was disposed of in landfills. With the size of landfills and their number rising, the need for plastic recycling and involving the product manufacturers in this process led to the introduction of the dual system, identifiable with the *Grüner Punkt* for consumers, in 1990 in Germany [38].

Since then, different national and international initiatives started to prevent the dumping the plastic litter in landfills and started to recycle the material. Nonetheless, is the amount of plastics recycled still very low, and effective waste management is not established in every part of the world. Therefore, a lot of plastic litter still enters the environment today. Most people are aware of these facts nowadays, and organisations, that want to mitigate the plastic waste in the environment or focus on retrieving the plastic that already entered the environment, e. g. *The Plastic Soup* [39] and *The Ocean Cleanup* [40] were founded.

Since many consumers and producers do not want to miss the advantages of plastic, products made of bioplastics are increasingly being offered, which are also intended to reduce the bad conscience when buying plastic products. The term bioplastic is not defined consistently. It can be plastic made from renewable raw materials (bio-based) or simply plastic that degrades much faster than conventional plastic (bio-degradable) [41, 42]. Since this degradation of the bioplastic

also results in the creation of micro- and nanoplastics, these do not necessarily count as a better alternative to conventional plastic. There are also some bioplastics, that are bio-based as well as bio-degradable, but the competition for raw materials with food production makes large-scale production ethically debatable. In addition, strict hygiene regulations apply to food packaging, which makes the use of recyclates and some bioplastics more difficult [43]. Therefore conventional plastic is still used very often in this area.

### 2.2.1 *Formation of micro- and nanoplastics*

Micro and nanoplastics (MNPs) are small plastic fragments. Microplastics are usually defined as pieces of plastic between 1 and 1000 µm in size, with earlier classifications setting the upper size limit at 5 mm. Nanoplastics, on the other hand, are particles that have a size of 1-1000 nm [44–46]. This limit differs from that of NPs, which only go up to 100 nm.

MNPs enter the environment due to two main reasons. Directly emitted plastic particles are called primary MNPs [47, 48] and can be fibres of washed clothes or can be found in cosmetics or modern sports fields. The other way of MNP emission is the breakdown of larger plastic debris. The MNPs that were formed by this degradation are called secondary MNPs [48, 49]. The breakdown of plastic particles can be divided into three main types:

1. mechanical degradation
2. chemical degradation
3. biological degradation

*Mechanical degradation*

The main mechanical stress, that leads to the formation of MNPs is abrasion [50]. Abrasion can occur when plastic particles are rubbed against natural items, i. e. sediment grains, shells, wood debris, stones, and rocks. Besides the abrasion on natural items, there are also man-made items, that contribute to abrasion through their contact with plastic. These objects are mainly vehicles or boats, and buildings. But the interparticular abrasion between two plastic particles or larger plastic debris can also take place. Additionally to the abrasion, temperature changes as well as the change between wet and dry periods also lead to degradation. When these mechanical degradation processes occur over a long period of time, the resulting plastic particles usually have a nearly-spherical shape, similar to the sediment particles [50, 51].

*Chemical degradation*

The chemical degradation depends very much on the chemical structure of the polymers and on potential additives. A main factor is UV radiation exposure (photodegradation) [52]. For polyolefins, PS and PVC, additives and impurities are helpful to break the C-C bonds [50]. PET, on the other hand, is already sensitive to photooxidation but can also hydrolyse in the absence of UV radiation (e.g. at the bottom of the sea) [53]. In polyolefins, besides photodegradation, thermal degradation can also break C-H bonds or eliminate side groups if the thermal energy is sufficient [52]. This creates free radicals that can react with oxygen and lead to chain breakage and crosslinking. Due to degradation, the polymer is more brittle, making it more susceptible to mechanical degradation [50, 52].

*Biological degradation*

For the microbial degradation of plastic debris, the presence of water is essential [50]. When in contact with water, a conditioning film of dissolved organic matter can form on the surface of the particle [54, 55]. The conditioning film of biomolecules, as well as cracks and indentations of the surface caused by the other types of degradation, offer the possibility for colonisation of the plastic surface by microbial communities. This is also called plastisphere [56]. The next step in microbial degradation is bio-fragmentation, which is performed by exoenzymes to break the polymer chains into oligomers. If the plastic debris is small enough to penetrate the tissue, the particles can serve as a carbon and energy source for microorganisms. This is called assimilation [57]. The microorganisms turn the solid plastic into carbon dioxide, water, and methane, which is called mineralisation [57, 58]. The biofilm on the surface of a plastic particle can also interact with the other types of degradation since the microorganisms can form protection against mechanical abrasion and also change the density and therefore lead to sinking in the water column [50, 54]. There are reported microorganisms that can degrade polyolefins [59–61].

The processes, that generate microplastic can also result in nanoplastic. Because of the similar formation processes when it comes to secondary MNPs, the research topics in micro and nanoplastic research usually overlap. Due to the much smaller size of nanoplastics, the properties and potential environmental and toxicological effects are different. Bacteria and other small microorganisms are very often larger than the nanoplastic particle and cannot colonise the particle surface, as they can do with microplastic surfaces.

## 2.3 METHODS

The detection and characterisation methods for environmental nanoplastic samples differ a lot from the methods used to characterise the potential reference materials. The first part of this method section is about the methods used to characterise the nanoplastic dispersions prepared, while the second part deals with a short overview of the methods used for environmental microplastics and nanoplastics and where they fail.

### 2.3.1 *Light Scattering*

When it comes to nanoplastic detection, dynamic light scattering (DLS) is a very strong method. It is a non-destructive method and can be applied in an easy and fast measurement setup. Therefore the DLS method was selected for the measurements of the reference material candidates because users can easily check the sample quality with a DLS instrument prior to the experiments. Light scattering is possible for dispersed systems with a particle size of less than 10 µm. The samples must be emulsions (liquid/liquid dispersions) or suspensions (solid/liquid dispersions). In both cases, the continuous phase of the sample is a liquid.

While static light scattering (SLS) is used to determine the molar mass of a dissolved polymer, dynamic light scattering detects the time-resolved diffusion of a particle in a dispersion. Diffusion, or more precisely the diffusion coefficient, is related to the hydrodynamic radius of a spherical particle via the STOKES-EINSTEIN equation written as

$$D = \frac{k_\mathrm{B} T}{6\pi\eta R_\mathrm{h}} \tag{2.1}$$

where the diffusion coefficient is $D$, the Boltzmann constant is $k_B$, the absolute temperature is $T$, the dynamic viscosity is $\eta$, and the hydrodynamic radius is $R_\mathrm{h}$.

In light scattering experiments, particles are irradiated with a laser beam, resulting in elastic scattering of light. This is normally detected at different angles. Figure 2.4 shows an example of the setup of a light scattering system.

The laser light hits the sample and gets scattered. The difference between the vectors of the incident light $\vec{k_0}$ and the scattered light $\vec{k}$ at the scattering angle $2\theta$, is the scattering vector $\vec{q} = \vec{k} - \vec{k_0}$. The modulus of $\vec{q}$ is defined as

$$q = \frac{4\pi n}{\lambda} \sin\theta \tag{2.2}$$

where the refractive index is $n$, the wavelength of the incident laser is $\lambda$, and half the scattering angle is $\theta$. In a standard DLS instrument,

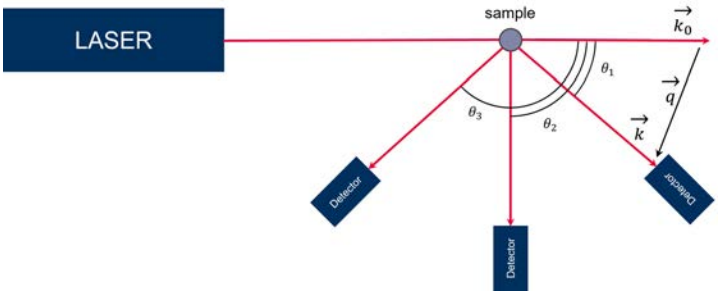


Figure 2.4: Schematic setup of a light scattering instrument. The laser light gets scattered at a sample. The scattered light is detected at different angles (here $\theta_1$, $\theta_2$, and $\theta_3$). The scattering vector $\vec{q}$ is the difference between the transmitted light $\vec{k_0}$ and the scattered light $\vec{k}$.

the detection usually takes place at a perpendicular (90°) or at a backward (173°-175°) scattering direction. Particle diffusion based on Brownian motion takes place on a nanosecond to millisecond scale. For these time intervals, the normalised autocorrelation functions are calculated according to

$$g_2(\tau) = \frac{\langle I(t)I(t+\tau)\rangle}{\langle I(t)\rangle^2} \tag{2.3}$$

where the scattering intensity at time $t$ is $I(t)$ and delay time is $\tau$. For small $\tau$ the maximum of $g_2(\tau) = 2$ and the minimum for larger $\tau$ is $g_2(t) = 1$. Therefore the reduced autocorrelation function $g_2 - 1$ is usually used. Besides the intensity autocorrelation function $g_2$ there is also the field correlation function $g_1(\tau)$. Both are connected via the SIEGERT relation, which is defined as

$$g_2(\tau) = 1 + \beta\,|g_1(\tau)|^2 \tag{2.4}$$

where $\beta$ is a factor representing the experimental geometry. The most common analysing method for the DLS experiment is the cumulant method. For this, the autocorrelation function is approximated as

$$g_1(\tau) = \exp\left(-\bar{\Gamma}\tau\right)\left(1 + \frac{\mu_2}{2!}\tau^2 - \frac{\mu_3}{3!}\tau^3 + \ldots\right) \tag{2.5}$$

where the average decay rate is $\bar{\Gamma}$ as the first cumulant, the second and the third cumulants $\mu_2$, and $\mu_3$ [62]. With the first cumulant $\bar{\Gamma}$ the hydrodynamic radius $R_\mathrm{h}$ can be determined via

$$\bar{\Gamma} = q^2\, D \tag{2.6}$$

$$R_\mathrm{h} = \frac{k_\mathrm{B}Tq^2}{6\pi\eta\bar{\Gamma}} \tag{2.7}$$

$\mu_2$ and $\mu_3$ can be used to determine the polydispersity of the sample. For samples with a rather low dispersity, the use of the second cumulant only can be more precise. Therefore, the Equation 2.5 was shortened for the analysis of multi-angle light scattering (MALS) experiments, following the suggestion of Frisken [62] to obtain better fitting results.

$$g_2(\tau) - 1 = B + \beta \exp\left(-2\bar{\Gamma}\tau\right) \left(1 + \frac{\mu_2}{2!}\tau^2\right)^2 \tag{2.8}$$

With the baseline $B$. The term $B$ different than zero can be helpful because, in the experimental setup, the minimum values of $g_2(\tau) - 1$ can slightly differ from zero. In general, the cumulant method leads to more stable results concerning possible background noise, etc. than other analysis methods (e.g. CONTIN algorithm [63]) and is very often the standard analysis in DLS instruments' software.

*Particle Concentration via DLS*

The latest MALS instruments and software make it possible to calculate the particle concentration in a dispersion. This is also a very helpful tool to determine the concentration of the prepared nanoplastic samples because other methods often fail. For this method, the detected count rate $(I_{\text{total}} - I_{\text{solvent}})$ at different scattering angles $\theta$ is analysed because every particle size class contributes to the scattering of the complete sample. The usual result of the analysis is the particle size distribution (intensity-weighted) $x(d)$. It is related to the particle concentration distribution $\rho(d)$ via [64]

$$\rho(d) = \frac{(I_{\text{total}} - I_{\text{solvent}})x(d)R_{\text{toluene}}}{I_{\text{toluene}}\frac{dC_{\text{scattering}}}{d\Omega}(d,\theta)} \tag{2.9}$$

The quotient $\frac{dC_{\text{scattering}}}{d\Omega}(d,\theta)$ is the differential scattering cross section and depends on the size $d$ and the scattering direction $\theta$. It can be calculated using the Mie theory with the properties of the scattering material, the continuous phase, and the experimental setup. To eliminate factors, that come from the instrument's setup etc, the reference solution of toluene is measured ($I_{\text{toluene}}$ as the count rate of pure toluene) and the Rayleigh ratio of toluene $R_{\text{toluene}}$ is used, which is known in the literature. The quotient of both equals a factor that normalises the measured count rate. Since several terms in Equation 2.9 are size-dependent, the particle size should be determined as precisely as possible to reduce errors and their propagation.

To calculate the number concentration of particles in the dispersion, it is necessary to measure the scattering at more than one scattering angle. The Mie scattering of larger particles ($> \lambda/10$), which has to be taken into account for the particle concentration distribution, is dependent on the scattering angle [65]. A basic single-angle instrument,

therefore, fails to give sufficient data to provide information on the concentration.

### 2.3.2 *Zeta Potential*

The zeta potential ($\zeta$) is also called electrokinetic potential. By means of electrophoretic light scattering (ELS), it can often be determined with the same instrument as DLS. The zeta potential determination deals with the surface properties of the dispersed particles and provides information about the stability of a dispersion. To achieve long-term stability, the surface of particles is often modified by chemical or physical processes. The best-known method is the addition of surfactants or polyelectrolytes to a dispersion to improve stability. In addition, due to their nature, particles can show a repulsive electrostatic interaction in the dispersion medium. This is the case for the prepared nanoplastic particles in this work. The determination of the zeta potential bases on the principles of colloidal stability, already discussed in Section 2.1.2.

The most commonly used method for the experimental determination of the zeta potential is electrophoresis. With the help of this method, dispersed particles of a size of 1 nm - 20 µm can be measured in a liquid medium. For this purpose, the speed with which the particles move when an electric field is applied is measured. One potential method for the calculation of the zeta potential is the one introduced by SMOLUCHOWSKI, which is defined as

$$\zeta = \frac{\nu_{ep}}{E} \cdot \frac{\eta}{\varepsilon_f \varepsilon_0} \tag{2.10}$$

where the electrophoretic velocity is $\nu_{ep}$, the electric field strength is $E$, the dynamic viscosity of the medium is $\eta$, the dielectric constant of the medium is $\varepsilon_f$ and the permittivity in vacuum is $\varepsilon_0$.

This equation applies only to particles that are not conductive and have a rather thin double layer $\kappa R >> 1$, with the DEBYE-HÜCKEL parameter $\kappa$.

For conductive particles and a thicker double layer ($\kappa R < 1$), the equation was modified by HÜCKEL as

$$\zeta = \frac{\nu_{ep}}{E} \cdot \frac{3\eta}{2\varepsilon_f \varepsilon_0} \tag{2.11}$$

Equation 2.10 is usually used when working with aqueous dispersions, as the double layer is usually thin here. For non-aqueous dispersions, however, the HÜCKEL Equation 2.11 is more appropriate theoretically.

### 2.3.3 *MNPs detection methods*

So far, detection methods for plastic particles in the environment mainly refer to microplastic particles. This is the case because these particles are much easier to detect due to their size. Microplastics are for the most part - in contrast to nanoplastics - observable to the human eye. What began with microplastic particles is now intended with successively smaller particles as well. This is significantly more difficult due to their smaller size and the general chemical composition of plastics. Because many methods overlap the field of microplastics and nanoplastics, this section briefly presents methods that are used for microplastic samples and to what extent they can also be transferred to nanoplastics. Because of the degradation mechanisms presented in Section 2.2.1 it can be assumed that nanoplastics are also present in the environment in addition to microplastics that have already been detected. There are MNPs in nearly every environmental matrix [6, 66, 67]. They are sampled in water, soil, air, and biota.

In general, the sampling method depends on the research question that is to be observed. In the field of microplastic sampling in waters, net sampling techniques are the predominant methods. These nets come in various setups and mesh sizes (mostly 50 - 500 µm). Therefore, only rather large plastic debris is collected. Smaller marine biota and water are usually excluded by this sampling method. Other material, that is not plastic (e. g. shell debris) is still collected together with microplastic. The different setups make vertical and horizontal sampling possible. The nets are linked to a flowmeter to estimate the water volume that flowed through the net. The net sampling does not work for nanoplastics. The main point is the mesh size which cannot be decreased to such an extent, that nanoplastics can be sampled efficiently without the water. Therefore, nanoplastic is usually sampled in bulk. This means a bottle, bucket, etc. is used to sample water from the surface or the water column. Nonetheless, the sampled volume is rather low and all kinds of small marine biota are still present in the sample and need separation. The bulk sampling methods for water can also be transferred to sedimental or snow matrices, while here the separation between sediment and plastic samples is even more elaborate.

Atmospheric MNPs can be sampled actively or passively. While active sampling includes the collection of dust in a room or the pumping of air through an adequate filtering system, passive sampling can be achieved with adhesive pads or a funnel that directs settling MNPs into a bottle, where they are collected. Finally, samples of marine biota are collected with nets or by purchasing them from local fishermen, etc. A more detailed overview of the different sampling methods, their advantages, and disadvantages as well as limitations are given in the review by Lai et al. [68].

After satisfactory sampling, the plastic needs to be extracted from the matrices. There are different procedures to separate plastic and other solid contents in the matrix. They usually include sieving/filtration, centrifugation/flotation, and purification via chemical treatment. Chemical treatment typically means the use of oxidants, enzymes, and strong acids or bases. Normally, a combination of all these chemical purification steps is combined. The executor has to be aware of the possible impacts on the plastic sample material, which these treatments can have. Until now, there is no standard way of processing environmental MNPs samples, because the matrices and the research objectives vary and may affect the treatment needed. The *National Oceanic and Atmospheric Administration* (NOAA) proposed a standard microplastic sample treatment procedure for water and sediment matrices [69] and there are proposals for a standard procedure for MNPs samples from animal tissue [70].

When the extraction of the MNPs was successful, the samples are ready for characterisation. There are non-destructive and destructive characterisation methods. Microscopy and its variations are non-destructive methods. The variations used for MNPs samples are electron microscopy (mostly scanning electron microscopy (SEM)), Fourier Transform Infrared (FTIR), and Raman microscopy. For larger MNPs normal light microscopy can be performed but is limited to the rather poor resolution of visible light for very small structures (Abbe diffraction limit). With the microscopic methods, the particle size, morphology, and with the help of vibrational (FTIR and Raman) microscopy the polymer type can be determined. The combination of spectroscopy and microscopy simultaneously provides information about the chemical structure of the particles (spectroscopy) and spatially resolved information about the particles, as well as their size (microscopy). The lower detection limit for MNPs in FTIR microscopy is 10 µm and ca. 1 µm in Raman microscopy [71]. Limitations in Raman microscopy result from the lower excitation laser energy (i. e. higher wavelengths) which prevents fluorescence but reduces the sample's signal [71]. Therefore microscopic methods mostly fail to identify nanoplastics. Only electron microscopic identification is possible for nanoplastics lower than 1 µm and was also used in this work.

Destructive methods usually involve the initial thermal decomposition of the samples and subsequent characterisation of the decomposition products. The methods to choose between are pyrolysis coupled with gas chromatography-mass spectrometry (Py-GC-MS) [72, 73] and thermal extraction desorption gas chromatography-mass spectrometry (TED-GC-MS) [74–76]. These methods identify the polymer type of the MNPs as well as their amount. They fail to give the exact size and shape of the particle. An advantage is the lower detection threshold, which also forgives an incomplete sample extraction.

The DLS method, described in Section 2.3.1 is not suitable for the detection of environmental nanoplastics. The DLS is very sensitive to small amounts of impurities. A single dust particle can interfere with the scattering of the plastic particles. Also, a large dispersity in particle size, which has to be expected in environmental samples, can complicate the analysis of the DLS results.

All things considered, the detection of environmental nanoplastics remains rather difficult. One limitation is the restricted detection methods that are useful for nanoplastics. The other limitation is the very low concentration of nanoplastics in the environment.

Besides physical limitations, most nanoplastic detection methods are only tested with nanoplastic particles that can be purchased and usually are not made for this specific use. Mostly, they are PS or PMMA nanospheres which are easier to produce but are not necessarily similar to those found in the environment. Therefore it makes sense to test detection methods for nanoplastics with nanoplastics reference materials that are as close to the environmental MNPs as possible.

# 3

# RESULTS AND DISCUSSION

The first part (Section 3.1) covers the preparation of nanoplastic dispersions made of polyolefins, PP and PE. Eventually, they are dispersed in water. The preparation follows a top-down method from the pristine plastic pellets or powder and was used to prepare a reference material candidate. Also, possibilities to stain the particles with precious metals for better detectability, especially in organic matrices will be discussed. The second part (Section 3.2) will focus on the preparation of nanoplastics, which are made of one of the most common biopolymers PLA. In contrast to the poorly soluble polyolefins, the PLA nanoparticles are prepared in a bottom-up strategy. Here, the possibility to stain the particles with gold as well is discussed.

## 3.1 POLYOLEFIN NANOPLASTICS

As discussed in Section 2.2, the polyolefins PP and the different types of PE take a huge part in the polymers produced worldwide every year. So far, there are no polyolefin nanoparticles available for researchers to use in their experiments. The first groups introduced ways of preparing nanoplastics made of polyolefins, but often the preparation is rather complicated [77, 78]. Besides the preparation, the stability (i. e. Zeta potential) needs to be lower $-20$ mV to be able to store the samples over a longer period of time, making it necessary to freshly prepare the samples every time. This is also not feasible for every research group working with MNPs and makes the comparability of results obtained with different batches and in different laboratories more difficult. Therefore, the preparation method was adapted and improved to have a nanoplastic dispersion, that can be prepared under simple conditions and show very similar results even with many batches. A large number of batches that are available for MNPs research can enhance the comparability of tests carried out at different institutes but can also test and calibrate the detection methods used for nanoplastic detection and characterisation methods [7].

### 3.1.1 *Preparation conditions*

Commercially available PP and PE were used to prepare the nanoplastics. Here, different polymers can be used.In the preparation process of the reference material candidates, PP pellets with a molar mass of $\bar{M}_n = 5\,000$ g mol$^{-1}$ and PE powder with a molar mass of $\bar{M}_n = 1\,700$ g mol$^{-1}$ were used.

In an adaption of the preparation of PS and PE nanoplastics introduced by Ekvall et al. [77, 79], the polyolefin nanoplastics were prepared with mechanical stress applied to the polymer pellets using an Ultra-Turrax® disperser. Here, the tool (S 18 N - 19 G) is mostly made of stainless steel (AISI 316L grade) and PTFE [80], reducing the possibility of plastic contamination from the tool to a minimum. Other changes in the preparations were made to obtain more stable polyolefin nanoplastics dispersions in water, such as the use of acetone for the mechanical stress step and the use of purified water as a solvent after solvent exchange. In the preparation, different masses of polymer and processing times, as well as dispersant volumes, were tested to find the most suitable setup for the reference material candidates. They will be discussed in the following. The polymer mass given here is the mass of the starting material. Not all macroscopic polymer was converted into nanoparticles, but there were also microscopic particles left, that were separated via simple filtration with a folded filter. All preparations were performed with PP pellets and the most promising conditions were applied to the preparation with PE powder.

Table 3.1: Overview of the resulting hydrodynamic diameter of nanoPP dispersions determined via DLS for different preparation conditions, comparing different processing times, polymer masses, and dispersant volumes.

| Time | 5 min | 10 min |
|---|---|---|
| $D_h$ (nm) | 146 ± 5 | 108 ± 3 |
| other parameters | polymer mass: 2 g | dispersant volume: 115 mL |
| Polymer mass | 2 g | 6 g |
| $D_h$ (nm) | 108 ± 3 | 128 ± 5 |
| other parameters | time: 10 min | dispersant volume: 115 mL |
| Dispersant volume | 115 mL | 345 mL |
| $D_h$ (nm) | 128 ± 5 | 133 ± 4 |
| $c_{PP}$ ($\mu g\ mL^{-1}$) | 26.8 ± 4.6 | 6.8 ± 1.4 |
| other parameters | polymer mass: 6 g | time: 10 min |

Table 3.1 shows, that for a constant amount of polymer pellets (2 g) present in the same dispersant volume (115 mL) a longer processing time of 10 min leads to smaller particles. The hydrodynamic diameter decreases from (146 ± 5) nm when the polymer debris is processed for 5 min to a size of (108 ± 3) nm when the time is extended to 10 min. This seems to indicate, that a longer processing time leads to more mechanical stress for each polymer particle and eventually

smaller particles, which is reasonable. The processing time was not further increased than 10 min due to the heating of the disperser from processing the polymer pellets. Another factor to consider is the amount of polymer, that is used in every batch. As a next step, the mass of the polymer was increased from 2 g to 6 g to see the effect on the resulting particle diameters.

When having a constant processing time and volume, a lower polymer mass of 2 g leads to smaller particles with a size of $(108 \pm 3)$ nm than the threefold mass of 6 g which results in particles with a size of $(128 \pm 5)$ nm. This can have two reasons. Firstly, when having fewer polymer particles present, each particle is processed with the disperser more thoroughly and the mechanical stress each particle is exposed to is higher compared to the higher polymer mass. Secondly, the concentration of the resulting particles probably depends on the concentration of the starting material. A higher concentration could decrease the stability of the dispersion and lead to an agglomeration of particles since no stabilising surfactant is present.
Because of this, the dispersant volume for the preparation with 6 g was increased to lead to an equivalent concentration as the 2 g preparation before. With a volume of 345 mL, the hydrodynamic diameter increased from $(128 \pm 5)$ nm to $(133 \pm 4)$ nm. When looking at the diameters including their errors, the sizes for different dispersant volumes do not differ significantly. Therefore, the concentration of the resulting dispersion does not influence the particle size, and a larger particle size comes more likely from the reduced mechanical stress, each polymer particle faces due to a higher amount of polymer. The time of applying the mechanical stress was not extended threefold, due to the reason mentioned above.

Nonetheless, the concentration of the nanoparticles changes in the dispersion, when higher polymer masses are used. Besides the difference between a concentration of $(26.8 \pm 4.6)$ µg mL$^{-1}$ for a dispersant volume of 115 mL and a concentration of $(6.8 \pm 1.4)$ µg mL$^{-1}$ for a volume of 345 mL, there is also a visible difference between the two dispersion in their turbidity. Because for possible applications, a higher concentration is more useful, the reference material candidates were produced with the conditions given in Table 3.2.

Table 3.2: Overview of the preparation conditions used for the reference material candidates made of PP and PE.

| Polymer mass | Processing time | Dispersant volume |
|---|---|---|
| 6 g | 10 min | 115 mL |

These conditions that were found to result in the most suitable dispersions were also applied to the preparation of PE nanoplastics. Nonetheless, the resulting dispersion was different from the results

obtained for PP. The nanoPE dispersion was more turbid than the nanoPP dispersion, indicating a higher particle concentration or a larger particle size or both. The dispersions of nanoPP and nanoPE are shown in Figure 3.1.

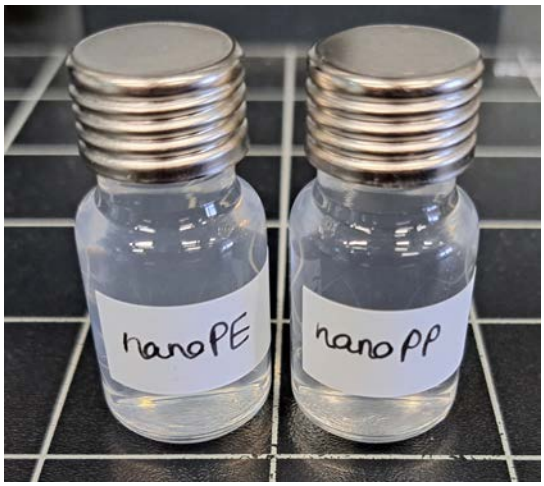


Figure 3.1: Photograph of the dispersions of nanoPE (left vial) and nanoPP (right vial) prepared under the conditions given in Table 3.2. The dispersion of the nanoPE particles is more turbid than the dispersion of nanoPP, which is due to the higher concentration and aggregates formed.

For the first experiments with a polymer mass of 2 g, a dispersant volume of 115 mL, and a processing time of 5 min, the resulting diameters for the nanoparticles were smaller for PE than for PP. At the same time, the concentration of the nanoPE particles is higher than the concentration of the nanoPP in dispersion. The concentration of the nanoPP dispersion was determined for a processing time of 10 min, therefore the concentration of nanoPP that was processed for only 5 min is presumably lower than $(19.6 \pm 3.3)$ µg mL$^{-1}$.

Table 3.3: Results of nanoparticle preparation with 2 g polymer, 5 min processing and 115 mL dispersant volumes for PP and PE. The hydrodynamic diameter of the resulting particles was determined via DLS and the particle concentration was determined gravimetrically. The concentration of the nanoPP dispersion was determined after a processing time of 10 min.

| Polymer type | PP | PE |
|---|---|---|
| $D_h$ (nm) | 146 ± 5 | 126 ± 6 |
| $c_{Polymer}$ (µg mL$^{-1}$) | 19.6 ± 3.3 | 31.7 ± 5.4 |
| polymer mass: 2 g | time: 5 min | dispersant volume: 115 mL |

The higher concentration at similar preparation conditions for PE led to an issue when scaling up the concentration for reference material candidate production. Here, the concentration of the nanoPE dispersion is ca. double the concentration of the nanoPP dispersion. The higher concentration affected the stability of the dispersion and probably led to larger particles due to aggregation and decreased colloidal stability as will be discussed in the following sections.

To ensure that only the size of the debris changes during nanoplastic preparation, but not the structure of the polymer, the molar mass of the polymers was determined before and after the application of mechanical stress using gel permeation chromatography (GPC). The results of the GPC experiments for PP and PE are given in Table 3.4. The data show that the molar mass does not change significantly in the process of mechanical stress. A slight change can be seen for the PE, but since the molar masses become larger here after processing and the dispersity does not change, it can be assumed that these are measurement inaccuracies due to the low molar mass. The dispersity of PP seems to change significantly with the process of mechanical stress, but this is only the reason because of the propagation of the slight change in the number-weighted mean molar mass, which leads to such a big difference in dispersity and therefore is negligible. With these results, it is demonstrated that in the developed preparation method of polyolefin nanoplastics, only the size of the particles but not their molar mass differs from that of the starting material.

Table 3.4: Number ($\bar{M}_n$) and mass-weighted ($\bar{M}_w$) mean molar masses of PP and PE and dispersity index Đ determined with GPC. For each sample, the molar mass was determined twice and the mean was calculated. The dispersity index was calculated from the quotient $Đ = \frac{\bar{M}_w}{\bar{M}_n}$.

| Sample | $\bar{M}_n$ ($g \cdot mol^{-1}$) | $\bar{M}_w$ ($g \cdot mol^{-1}$) | Đ |
|---|---|---|---|
| pristine PP | $1.1 \cdot 10^4$ | $3.6 \cdot 10^4$ | 3.3 |
| processed PP | $1.2 \cdot 10^4$ | $3.6 \cdot 10^4$ | 2.9 |
| pristine PE | $3.8 \cdot 10^3$ | $9.0 \cdot 10^3$ | 2.3 |
| processed PE | $4.0 \cdot 10^3$ | $9.2 \cdot 10^3$ | 2.3 |

The nanoplastic prepared under the conditions described in this section has a rather low molar mass. This molar mass was chosen, because it also represents the nanoplastic, that is not only mechanically degraded to nm scale in the environment but also faced chain scission, etc. (see Section 2.2.1) and is, therefore, a good representative for nanoplastic formed and found in the environment. However, the preparation was also performed with PP pellets with a higher molar

mass of $\bar{M}_n = 67\,000$ g mol$^{-1}$. This preparation led to similar results, which are shown in Figure 3.2.

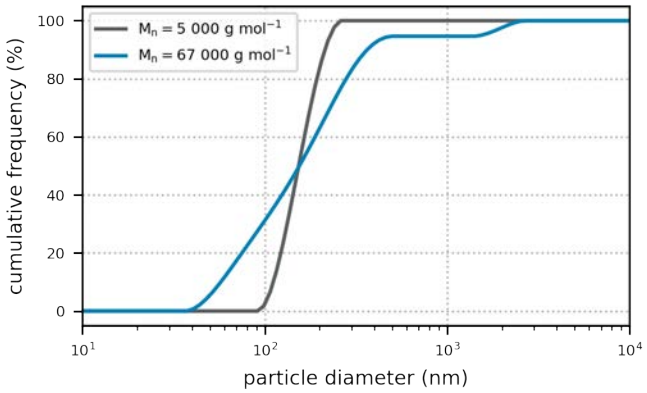


Figure 3.2: Cumulative frequency of the intensity of DLS measurements performed for two dispersions of nanoPP with different molar masses. $\bar{M}_n = 5000$ g mol$^{-1}$ (grey line) shows a single sharp distribution while the results for $\bar{M}_n = 67000$ g mol$^{-1}$ (blue line) show a broader distribution with an additional population at larger particles sizes in the micrometre range.

Both measurements were performed with an unfiltered sample. That is the reason for the population with a size of ca. 2 µm for the nanoPP dispersion with a higher molar mass (blue line). The sample with a higher molar mass also shows a broader distribution than the nanoPP dispersion with a lower molar mass (grey line). The main distribution starts at ca. 40 nm up to 500 nm. Both samples have in common that the sum of all intensities of the particles smaller than 150 nm is the same as the intensities of all particles larger than 150 nm. Because the light scattering intensity depends on the size (i. e. radius $r$) of the scattering object with $I \propto r^6$. This leads to a much higher scattering intensity for larger particles, in comparison to their number concentration present in the sample. Therefore the 2 µm population represents a rather low number concentration in comparison to the smaller particles present in the sample. All in all, the experiment shows that nanoplastic particles are also produced with a higher molar mass. The width of the size distribution differs from that of the particles with lower molar mass, but the preparation conditions were not adapted to the other starting material and could still be improved. This means, that the preparation method presented here can serve as a model for the production of nanoplastic dispersions from polyolefins. Depending on the desired property of the product, the preparation can be customised.

### 3.1.2 *Colloidal Stability*

The dispersions are stable without further stabilising surfactants as mentioned before. This is a surprising fact, considering the sole pres-

ence of polyolefin particles in water. Because no sterical stabilisation is expected for the particles, they have to be electrostatically stabilised to result in a colloidally stable dispersion. To investigate this assumption further, the zeta potential of the dispersions was examined. This is possible as electrophoretic light scattering in combination with dynamic light scattering on some instruments and with suitable cuvettes. The zeta potential of the dispersion turned out to be strongly negative. To be sufficiently stabilised in a sole electrostatic way, a minimum of $\pm$ 30 mV is required [81]. This indicates, that the dispersions of nanoplastic in purified water can be stable for a certain period. Previous work on the $\zeta$ potential of hydrophobic fluids in an aqueous environment showed, that the $\zeta$ potential here is negative in contrast to the expectation [82]. The reason they give for this negative zeta potential, is the adsorption of hydroxide ions on the hydrophobic surface [82, 83]. It has also been investigated for the interface of a Teflon or polypropylene film in water [84]. Investigating the $\zeta$ potential of the aqueous dispersions at different pH values, the $\zeta$ potential changes and shows a sigmoidal dependence. This is the case for both polymer types, which is shown in Figure 3.3. The sigmoidal fit follows

$$\zeta = \frac{\zeta_s K}{c(\mathrm{H3O^+})^n + K} = \frac{\zeta_s K}{10^{-n\mathrm{pH}+K}} \tag{3.1}$$

where $\zeta_s$ is the maximum $\zeta$ potential at the highest pH values, $K$ is the acid-base equilibrium constant and $n$ an exponent. The function was extrapolated to lower pH values, resulting in $\zeta$ potentials of 0 mV. When the measured $\zeta$ potential approaches values close to 0 mV, the colloidal stability of the dispersion fails and positive $\zeta$ potentials are not detectable with the applied method ELS in this case. The results for the application of Equation 3.1 for the nanoPP and nano PE dispersions are given in Table 3.5 and are shown in Figure 3.3.

Table 3.5: Parameters of the fit function Equation 3.1 for the zeta potential of nanoplastic dispersions measured at different pH values.

| | $\zeta_s$ (mV) | $K$ | $n$ |
|---|---|---|---|
| nanoPP | $-32.5 \pm 0.9$ | $(9.9 \pm 9.8) \cdot 10^{-6}$ | $1.3 \pm 0.1$ |
| nanoPE | $-43.8 \pm 1.3$ | $(4.7 \pm 1.5) \cdot 10^{-3}$ | $0.5 \pm 0.04$ |

The red dashed lines in Figure 3.3 represent the point of half titration. As well as the $\zeta$ potential of saturation $\zeta_s$ the point of the half titration is similar for both dispersions.
The nanoplastic dispersions were prepared with purified water to study their behaviour without the influence of possible contaminants in the dispersion medium. Even though, the purified water favours the extended colloidal stability of the dispersion and makes them therefore suitable as reference materials, nanoplastics in nature do

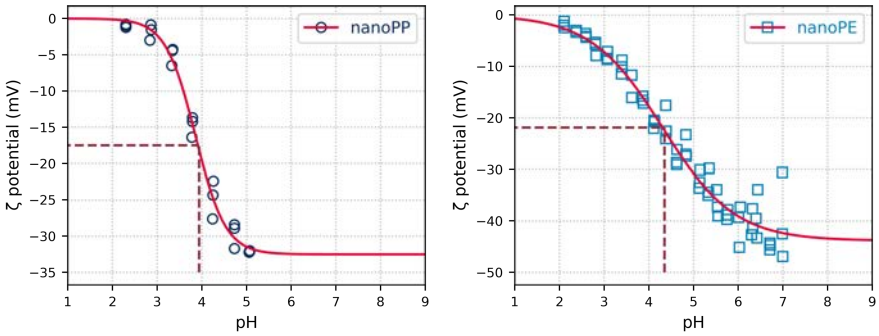


Figure 3.3: $\zeta$ potential at different pH values and sigmoidal fit. Left: Titration of a nanoPP dispersion towards lower pH with hydrochloric acid. Right: Titration of a nanoPE dispersion towards lower pH with hydrochloric acid.

not occur in a purified medium. For this purpose, their stability on a different medium was investigated. A normal saline solution of 0.9% NaCl and a saline solution with 0.09% NaCl in water were chosen. For testing the nanoplastic dispersion was mixed with NaCl to obtain the right concentration. DLS measurements were started directly after mixing the pristine particles with NaCl solutions in a volume ratio of 1 to 1. The colloidal stability of the dispersion was observed with a serial DLS measurement. The results are shown in Figure 3.4.

The experiments show that the hydrodynamic diameter determined for the nanoPP dispersion increases with time when the dispersant is a saline solution. Because an increase in the salt present in the dispersion decreases the stability of the dispersion decreases and eventually larger particles are formed by aggregation. This is the case for both, nanoPP (Figure 3.4 top) and nanoPE (Figure 3.4 bottom), but the stability of the nanoPE decreases faster. Furthermore, the formed structures are much larger than the particles that were formed for nanoPP, since the curves for 38 and 47 min do not reach 100% of the cumulative distribution function (cdf) for the normal saline concentration (a). For the lower saline concentration (b), the aggregation of particles takes place to a lower extent, since the cdfs rise more steeply, also for the later detection times, indicating a higher amount of smaller particles.

The fit applied to the cumulative distributions for monomodal and bimodal distributions follows

$$f(D_h) = \sum_{i=1}^{n} \frac{a_i}{n} \mathrm{erf}\left(\frac{\log\left(\frac{D_h}{D_{h,i}}\right)}{\sqrt{2}w_i}\right), \tag{3.2}$$

with $n = 1$ for $c_{\mathrm{NaCl}} = 0.9\%$ and $n = 2$ for $c_{\mathrm{NaCl}} = 0.09\%$. The $a_i$ represents scaling factors, which are a measure of the fraction of particle population $i$, respectively and the $w_i$ is the width parameter. The results of the fits are plotted in Figure 3.5. The blue curves represent

the agglomerated, larger particles, while the black curves represent the smaller particles, originally prepared.

While for both nanoplastics the diameter of the agglomerated species increases for the normal saline Figure 3.5(a) environment, they show a smaller increase and smaller agglomerates for the 0.9% saline Figure 3.5 (b). While the larger agglomerates form, the size of the median non-agglomerated particles slightly decreases. The insets of (b) show, the fraction of the larger and smaller particles over time. While the transformation for nanoPP (top) is nearly complete, the transformation for nanoPE is ca. 1:1. Nonetheless, the shorter measurement time for nanoPE has to be taken into account.

### 3.1.3 *Reference material preparation*

The aim of the project described in this chapter was to find a way to prepare reference material candidates made of polyolefins, to enhance the comparability of different nanoplastic studies. Here, a sufficient sample volume is needed to be able to perform many comparable experiments with the same material. To have a sufficient number of batches, the preparation of the nanoplastic dispersions needs to be scaled up. A higher dispersant volume, a higher polymer mass, and a longer processing time were not possible because of the aforementioned reasons. The nanoplastic preparation was carried out 60 times under the conditions given in Table 3.2 for each polymer type (i. e. PP and PE) and an aliquot of the resulting 115 mL batches were analysed with DLS/ELS. The results were checked for repeatability. All 60 batches contained nanoplastics. The measurands analysed were the hydrodynamic diameter $D_h$, the polydispersity index PDI (both measured at 175°) and the $\zeta$ potential. The mean $\mu$ and standard deviation $\sigma$ of all 60 samples were determined for each of the three measurands. A threshold of $\mu \pm 2\sigma$ was defined for identifying outliers. This is a compromise between a sample that is as homogeneous as possible and a sufficiently large sample volume. Figure 3.6 gives the measured values of diameter, PDI and $\zeta$ potential for PP and PE and the accepted range of $\mu \pm 2\sigma$ as green area. Every sample with a result beyond the range of $\mu \pm 2\sigma$ (reddish area) was excluded from the further reference material preparation.

After completing the first tests of repeatability, the batches, that lay in the green range only for all three measurands, were mixed in a big bottle ($V = 5$ L). Herein, the dispersion was mixed by swirling the bottle. Then, 10 mL aliquots of the dispersion were poured into smaller glass vials, the final reference material batches. This volume was considered to be an appropriate sample volume for nanoplastic testing. In total, 481 samples (for nanoPP) and 455 samples (for nanoPE) of 10 mL were obtained. The number for PE is a little lower because more batches were discarded.

To make sure, that these reference material candidate batches have similar characteristics, a sample of 20 samples were randomly chosen to determine the mean diameter, PDI and $\zeta$ potential of all reference material batches. Besides finding the mean and standard deviations of all measurands, this testing is also important to check the homogeneity of all batches. This is important, to make sure that all batches of the reference material (candidate) have similar characteristics. Here, a homogeneity study following the ISO guide for reference materials was performed [86]. The 20 batches were measured on three days with a different random order for each day to exclude potential trends in the results that derive from the measurement order only. An exemplary result of the DLS measurements of the nanoPP and nanoPE reference material candidates is given in Figure 3.7 as a size distribution. When filtered for the sample preparation, the DLS measurements result in only a single peak with a rather small peak width. The maxima for these samples are at $D_\mathrm{h} = 167$ nm for the nanoPP and $D_\mathrm{h} = 151$ nm for the nanoPE dispersion. For the nanoPP, the results do not differ much, for filtering or not filtering the samples with a syringe filter during the DLS sample preparation. For the nanoPE however, this is not the case. The results differ if the sample was filtered or not in the measurement preparation process. A test of homogeneity was performed for the filtered and the unfiltered reference material candidate, in this case, to evaluate, if filtering the sample with a syringe filter is necessary to obtain a comparable homogeneity of the dispersion when used in experiments.

For the $3 \times 20$ results for each measurand (size, PDI and $\zeta$ potential), analysis of variance (ANOVA) was performed to check if the means of the three datasets differ significantly. The detailed results can be found in the appendix (Table A.1 - Table A.9).

Table 3.6: Mean and standard deviation of $D_\mathrm{h}$, PDI, and $\zeta$ potential as a result of the homogeneity studies for nanoPP and nanoPE, when filtered and not filtered for sample preparation.

| | nanoPP | filtered nanoPE | unfiltered nanoPE |
|---|---|---|---|
| $D_\mathrm{h}$ (nm) | 180.5 $\pm$ 5.8 | 164.5 $\pm$ 19.3 | 344.5 $\pm$ 34.6 |
| PDI | 0.08 $\pm$ 0.02 | 0.19 $\pm$ 0.06 | 0.39 $\pm$ 0.04 |
| $\zeta$ potential (mV) | $-43.0$ $\pm$ 2.0 | $-37.9$ $\pm$ 2.0 | $-40.0$ $\pm$ 4.2 |

The results in Table 3.6 show, that the mean hydrodynamic diameter and especially the polydispersity index (PDI) of the nanoPP particles measured with DLS have only a small standard deviation. The PDI is below 0.1, which is believed to be highly monodisperse [65]. For the nanoPE particles, the DLS measurements lead to sizes, that show a standard deviation that equals ca. 10% of the mean, which is rather

high. The higher PDIs of the nanoPE dispersion for both sample preparation methods, support the suggestion, that the higher concentration of nanoparticles present in the reference material candidate, can lead to the formation of agglomerates. With a PDI of $0.1 - 0.4$ the samples are both moderately disperse [65]. However, the mean $\zeta$ potential of all three homogeneity studies is strongly negative and ensures the stability of the dispersions. The one-way ANOVA tests for all measurands were positive (i. e. null hypothesis accepted) but for the $\zeta$ potential of the filtered nanoPE dispersion (see appendix Table A.1 - Table A.9). Therefore, depending on the desired application for the nanoplastic reference material, the nanoPE dispersions can be used filtered and not filtered, resulting in a different size population of the particles.

The particles were also analysed using scanning electron microscopy (SEM). A micrograph of the nanoPP reference material candidate is shown in Figure 3.8. The particles are not spherically shaped, but with the applied mechanical stress, this was not to be expected. Furthermore, these irregularly shaped particles represent the nanoplastic found in nature more exactly than usually used commercial nanospheres do.

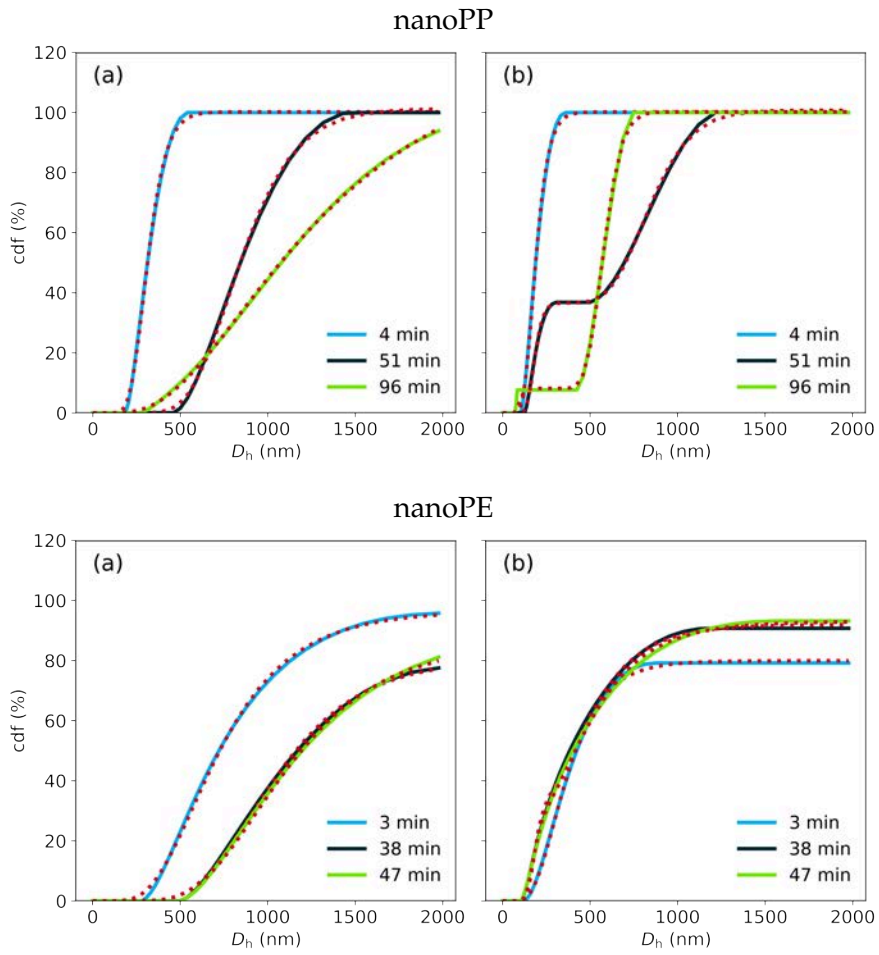


Figure 3.4: Serial DLS experiment of nanoplastics in saline. Time evolution of the cumulative distribution function (cdf) of the hydrodynamic diameters during storage. Displayed are cdfs for incubation times of 4 min (blue), 51 min (black), and 96 min (green) for nanoPP (top [85]) and 3 min (blue), 38 min (black) and 47 min (green) for nanoPE (bottom). Curve fits according to Equation 3.2 are provided as red dotted lines. Saline concentrations: a) $c_{NaCl} = 0.9\%$. b) $c_{NaCl} = 0.09\%$

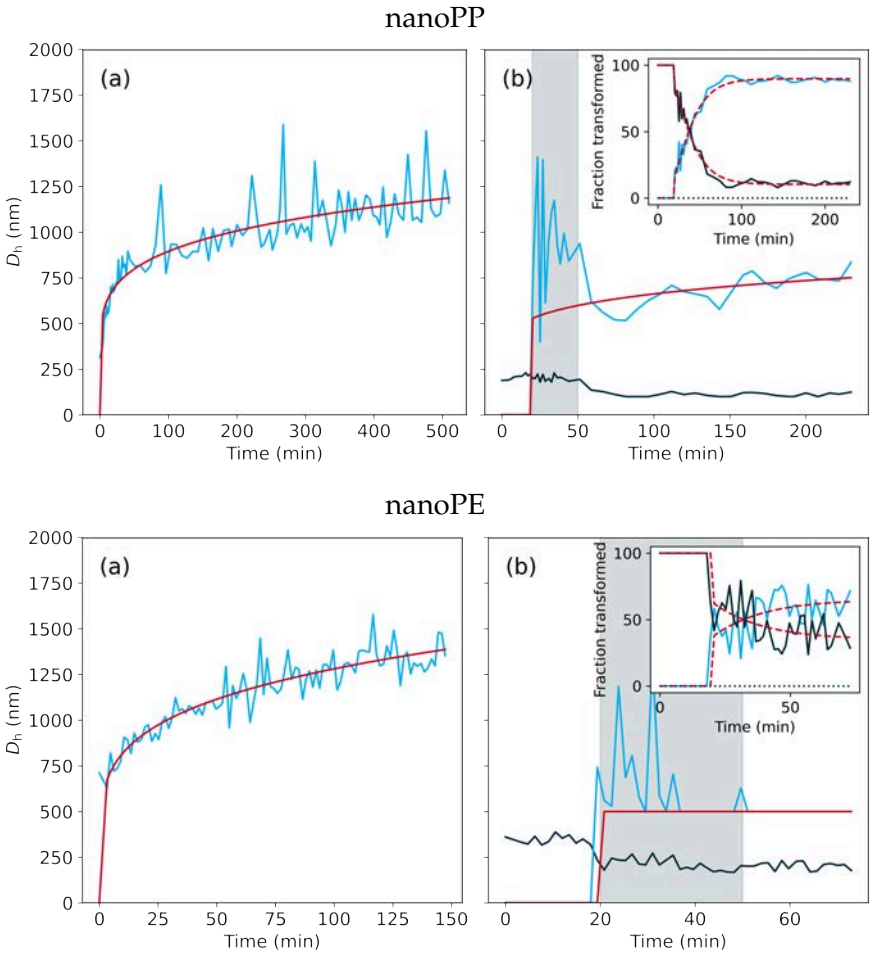


Figure 3.5: Median hydrodynamic diameters of nanoPP (top [85]) and nanoPE (bottom) at salt concentrations of a) $c_{NaCl} = 0.90\%$ and b) $c_{NaCl} = 0.09\%$ over the time of serial measurements. Inset: Fraction of particles transformed to larger agglomerates (blue) and non-agglomerated particles (black). Curve fits accordingly are given as red dashed lines.

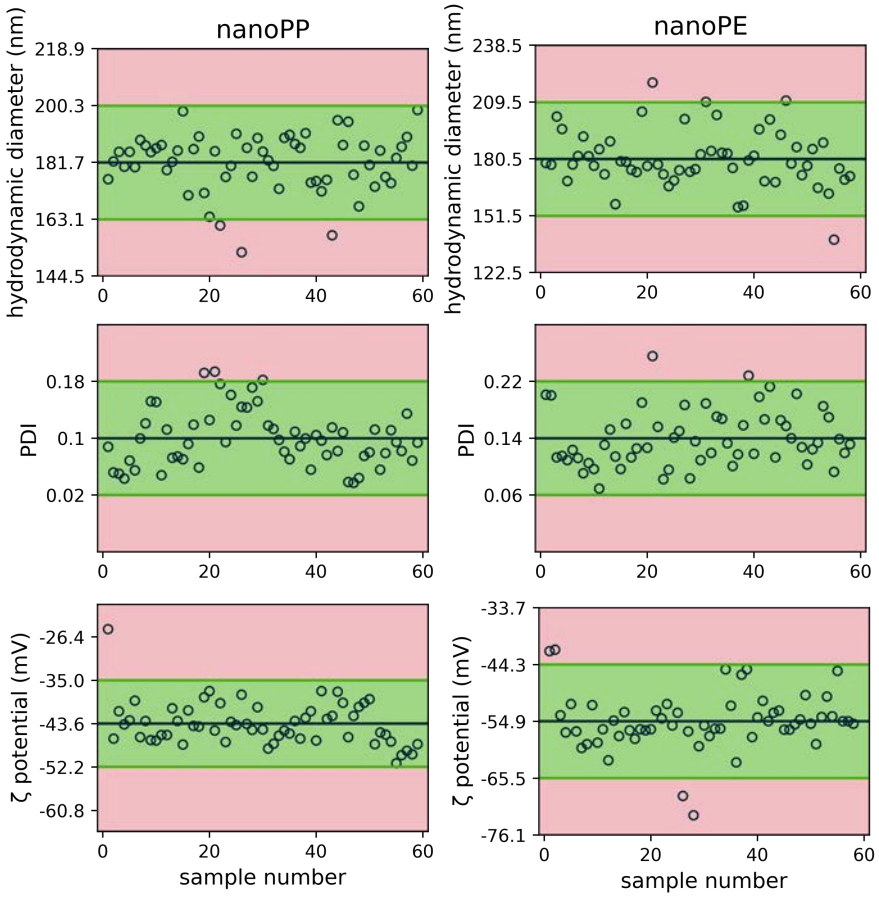


Figure 3.6: Results of DLS/ELS measurements for all 60 samples of nanoPP and nanoPE prepared. Each circle represents a sample. The green area represents a range of $\mu \pm 2\sigma$ which was accepted for reference material preparation and the red area represents a range of $\mu \pm x$ with $x < 2\sigma$. Samples with at least one measurement value in one of the red ranges were discarded and not used for the reference material preparation.

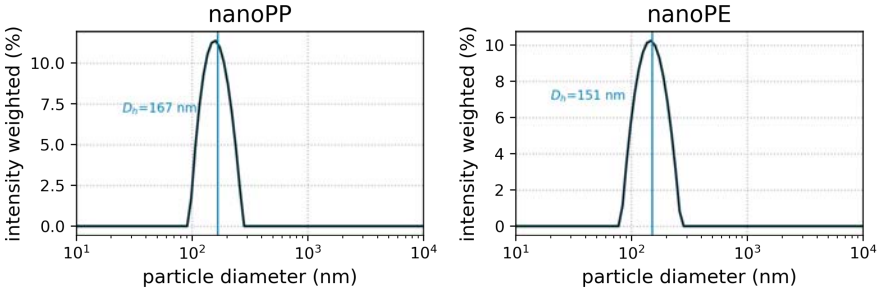


Figure 3.7: Intensity weighted size distribution of aqueous dispersions of nanoPP and nanoPE of the reference material candidates,

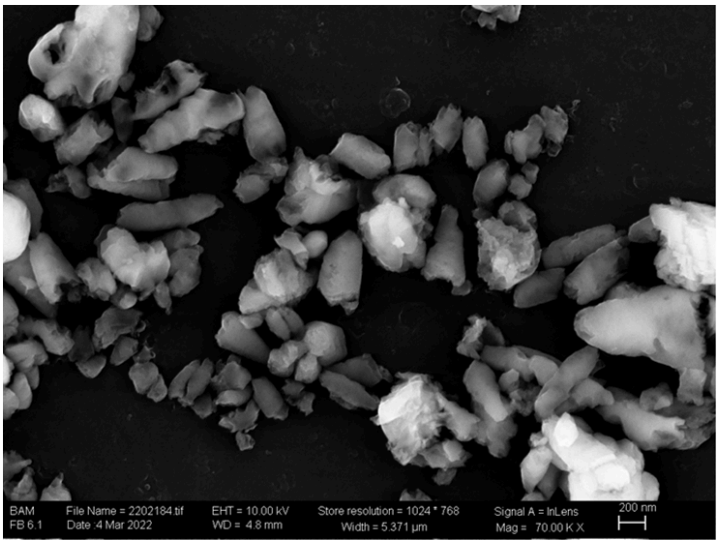


Figure 3.8: Scanning Electron Micrograph of nanoPP reference material. Scale bar = 200 nm [85].

### 3.1.4 *Gold-containing nanoplastics*

The disadvantage of polyolefin nanoplastics for toxicological applications is the similar chemical structure of the plastic and organic material, such as for example cells, etc. Therefore, they need to be stained to enhance the particle contrast in biological media. One possibility is using fluorescent dyes, like Nile red, that can be detected in light microscopy. Another possibility is using precious metal (nano)particles to include them in the particles. Gold is not a naturally occurring trace element in the body. At the same time, gold can be easily distinguished from organic material due to its high density, etc. Other precious metals, such as platinum, have already been used as a staining material for nanoplastics.[87] However, most of the time, the metal is incorporated in a bottom-up synthesis strategy.
Because the top-down approach has given evidence to be an easy and repeatable way to prepare PP and PE nanoplastics in dispersion, a way to dope the particles in this method was sought. In analogy to introducing additives (including dyes) to plastics by extrusion, the gold (in the form of salt $HAuCl_4 \cdot 3\ H_2O$) was added to the fully melted polymer. The polymer used has a relatively low molecular mass and therefore shorter polymer chains, resulting in a more liquid melt than higher molecular masses and making it easier to treat with the salt on a lab scale (i.e. without an extruder). The orange salt dissolved in the melted polymer. The colour turned from clear to brown. The water molecules of the trihydrate evaporate. The polymer turns a uniform brown colour when stirred. Then the polymer is cooled and it solidifies again. This preparation was carried out with two different amounts of gold salt, resulting in PP with a gold content of 0.1% and 0.5% (m/m). Figure 3.9 shows the stained polymers with different gold contents.

Figure 3.9: Photograph of the PP with increasing gold content. Left: pure PP prepared without gold salt; Centre: PP with a gold content of 0.1% gold; Right: PP with a gold content of 0.5% gold.

The photograph shows that the lower gold content (0.1%) results in a light brown colour, while the higher gold content (0.5%) results in a much darker colour. The colour of the pure PP that was melted and solidified again stays colourless like the starting PP pellets.

The obtained plastic was characterised. The small angle X-ray scattering (SAXS) experiments performed on these structures gave evidence of the crystalline structures of the polymer and the size of the added gold particles. With the used instrument and setup, also the wide-angle X-ray scattering (WAXS) range was detectable. Here information about the samples analogous to that obtained by X-ray diffraction can be obtained. With a equation similar to 2.2 the X-ray scattering vector $q$ can be transformed into the diffraction angle $2\theta$

$$q = \frac{4\pi}{\lambda} \sin\left(\frac{2\theta}{2}\right) \tag{3.3}$$

with the wavelength of the Cu $K_\alpha$ radiation $\lambda = 0.154$ nm used for these measurements. The refractive pattern of crystalline, isotactic PP can be found in literature [88]. The relevant $q$ section of the WAXS measurements performed for the PP samples is shown in Figure 3.10.

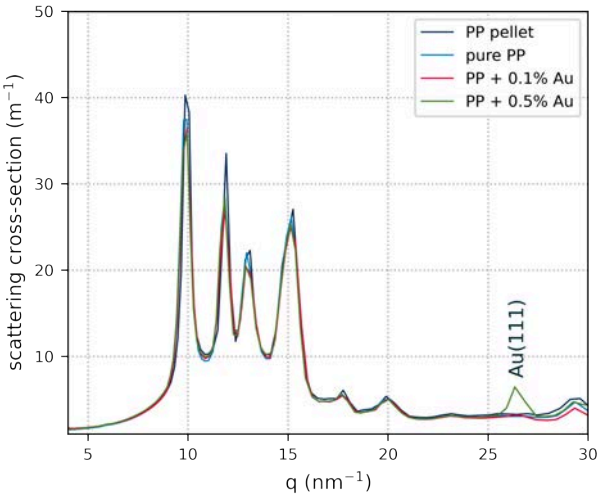


Figure 3.10: WAXS data of the scattering measurements performed for PP pellets (dark blue), pure PP (light blue), PP with 0.1% gold (red) and PP with 0.5% gold (green). For better comparability, the axes are in linear scale.

The curves of all samples overlap over most of the zoomed-in $q$ range. The first four, intensive peaks from $q$ = 10 nm$^{-1}$ to 15 nm$^{-1}$ represent the reflections of the crystalline, isotactic PP. The only larger difference is found at $q$ = 26.4 nm$^{-1}$, which occurs for the PP with a higher gold content only. This peak corresponds to the Au(111) plane. (For a more detailed analysis of the peak, see the section in the Appendix A.)

This peak gives evidence, that a crystalline gold structure is present in the plastic. The Au(III) was therefore reduced to Au(0) in the process of doping the melted polymer. This was expected since gold is an easily reducible metal and only harsh conditions (aqua regia) can oxidise elemental gold. At the same time, the hydrocarbon chains of PP can be slowly oxidised under environmental conditions, which is also a reason for MNP formation (see Section 2.2.1). This is the reason for the stabilising additives usually used in polyolefin manufacturing [89, 90]. The observed results are consistent with the expectations known from other reactive behaviour. However, the detailed reaction mechanism of gold is not the scope of this work, because the exact composition of the additives in the polyolefins is not known.
Because the baseline of the SAXS curve of the sample of PP with a lower gold content is a little lower here than the baseline of the pure PP, a smaller peak for the lower gold content can not be identified. However, the signal equivalent to the reflection of the Au(111) plane shows, that reduced gold atoms are present in the polymer, which will enhance the detectability of the gold since the reduced gold will hardly be dissolved in many solvents. However, not all reducing methods necessarily lead to gold NPs. Therefore, the size of the gold in the PP is of interest when characterising the obtained material. Previous work showed, that gold NPs can be incorporated into a 3D-printed plastic object [91] and show a brownish colour similar to the plastic obtained with this staining method (see Figure 3.9). A look at the remaining $q$ range of the SAXS curves can give an indication of the size of the gold within the PP.

Figure 3.11 shows the SAXS results for the three different PP samples. All of them show a population at an apparent radius of 6.6 nm, which results from the lamellar structure and the crystallites, that can be observed for PP [92, 93]. The size distribution of this population does not differ significantly for all three samples, indicating, that the doping with gold does not affect the structure of the solid polymers.

The other population at a radius of ca. 110 nm in the size distribution, which can be especially observed for the PP with a higher gold content represents the gold present in the polymer. With analysing the Au(111) peak in the SAXS data using the SCHERRER equation [95], the size of the crystallites in the gold particles can be determined. A more detailed calculation is given in the Appendix A. The size of the single crystals is 0.98 nm, which means, polycrystalline structures were formed. However, with the present sample preparation, no large single crystals were expected either, since producing large gold single crystals usually requires close monitoring of temperature and other process parameters, as e. g. in the BRIDGMAN [96] or the CZOCHRALSKI [97] method. The exact structure of the particles remains unclear, due to the heavily structured scattering curve of PP.

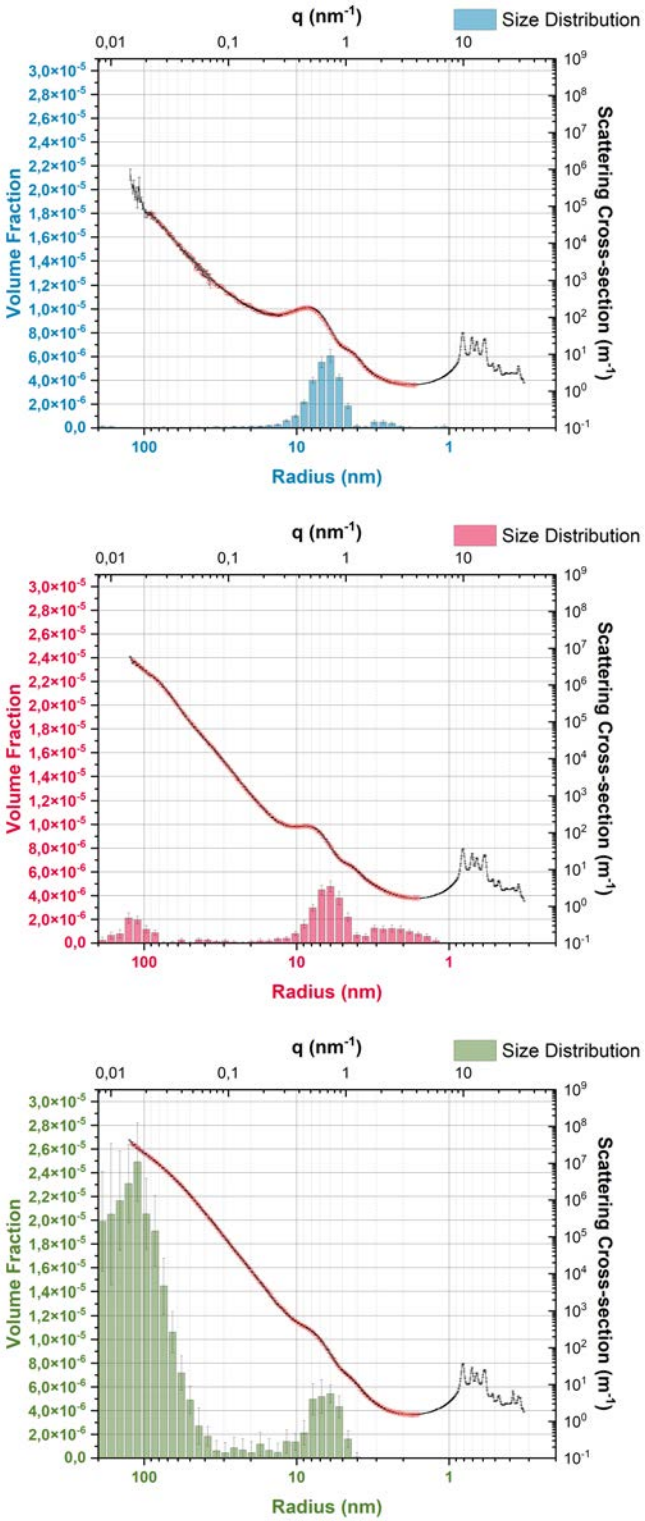


Figure 3.11: Results of the X-ray scattering experiments for PP with increasing content of gold from the top (light blue = pure PP) to red in the middle (0.1% gold) to the bottom (green = 0.5% gold). The results show the SAXS and WAXS measured with the MOUSE instrument [94]. The data (black) was curve-fitted (red line) in the SAXS range. The resulting size distributions are shown as radius-dependent histograms.

Since the mean radius of the particles is around 110 nm, the particles do not count as nanoparticles, which is not of the utmost importance for the planned scope of application. Additionally, the sub-micron particles are not of uniform size and show a rather broad size distribution, which could be expected from the preparation procedure applied. Again, this fact does not affect the suitability of the material for further applications.

The nanoplastic preparation method discussed in the section before was also performed with the gold-containing PP. The mass of the polymer pellets was reduced to $m = 2$ g due to the reduced amount of polymer stained with gold. The preparation resulted in aqueous dispersions of nanoPP with a gold content of 0.1% and 0.5%. These dispersions are shown in Figure 3.12.


Figure 3.12: Photograph of vials containing the gold-stained nanoPP particles dispersed in water. Left: NanoPP dispersion prepared with the PP containing 0.1% gold. Right: NanoPP dispersion prepared with the PP containing 0.5% gold.

Comparing the optical appearance of the two dispersions, it is noticeable that the dispersion of the nanoparticles with the higher content of gold is more turbid than the one with the lower gold content in the nanoparticles. Reasons for higher turbidity are, on the one hand, the presence of larger particles in the dispersion and, on the other hand, a higher particle concentration also leads to higher turbidity, as the light is scattered more strongly in these cases. In addition, the dispersed material's optical properties (in this case, the refractive index) can change turbidity. In this case (since the starting material of the two dispersions is not the same), all of the reasons mentioned for higher turbidity can come into effect. Therefore, the dispersions were examined as usual by light scattering. The resulting size distributions of the nanoparticles are shown in Figure 3.13.

Both size distributions show only a single population with a relatively small width. The mean hydrodynamic diameter $D_h = (107.5 \pm$

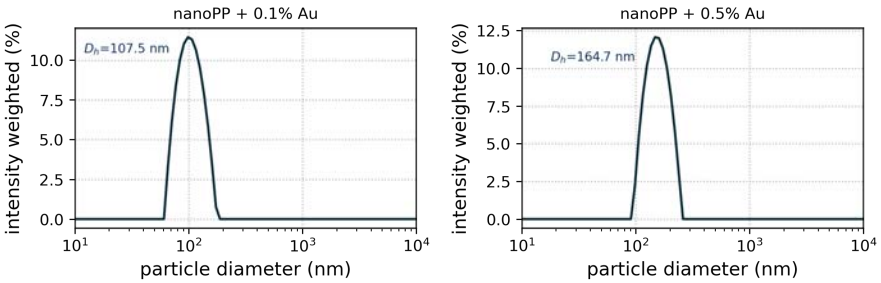


Figure 3.13: Intensity weighted size distributions of aqueous dispersions of nanoPP with a gold content of 0.1% (left) and 0.5% (right). The mean hydrodynamic diameter $D_\mathrm{h}$ are 107.5 nm (0.1% gold) and 164.7 nm (0.5% gold).

25.6) nm for the lower gold content and $D_\mathrm{h} = (164.7 \pm 37.6)$ nm for the higher gold content show, that the preparation method led to nanoplastics and their size differs only slightly. Especially the nanoPP with the lower gold content does not differ in size from the nanoPP that was produced without gold but under the same conditions (see Table 3.1).

The dispersions were also analysed using X-ray scattering. Because of their size and the low concentration of the nanoparticles, measuring the dispersion, even with higher concentrations was not successful, using the MOUSE instrument. Therefore, the sugar trehalose was added to the dispersions and then they were freeze-dried, leaving a mixture of gold-containing nanoplastic particles in trehalose sugar. Trehalose has been extensively used as a cryoprotectant for several decades for very sensitive structures, such as cells etc. [98, 99]. The results of the SAXS measurements are shown in Figure 3.14.

The X-ray scattering curves of the nanoplastic particles in trehalose all have a rather broad peak ("bump") in the wide-angle scattering range which comes from the freeze-dried trehalose. In contrast to the untreated samples in Figure 3.11, no information on the crystalline structure of the sugar can be obtained in this region of the scattering vector. The sample, that contains the nanoPP reference material in trehalose (light blue) shows two distinct populations when the size distribution analysis is performed. The first, smaller population from 11 to 85 nm radius with a rather low intensity represents the nanoplastic particles. The population at larger radii ($> 130$ nm) presumably represents the trehalose, which has not been subtracted from the SAXS data. Furthermore, there are populations with a higher frequency present in the other two SAXS results for gold-containing particles. In these samples, however, no difference can be detected between two, differently sized and intensive populations. The distribution here already starts at radii of less than 100 nm (25 nm for 0.5% Au and 45 nm for 0.1% Au). It can therefore be assumed that the populations of trehalose and the gold-labelled particles overlap. Since the samples

were measured as powders, the form factors play a major role in the final result. This was further complicated by the added gold, which means that no precise distinction can be made between gold particles, nanoplastic particles and trehalose as a cryoprotectant.

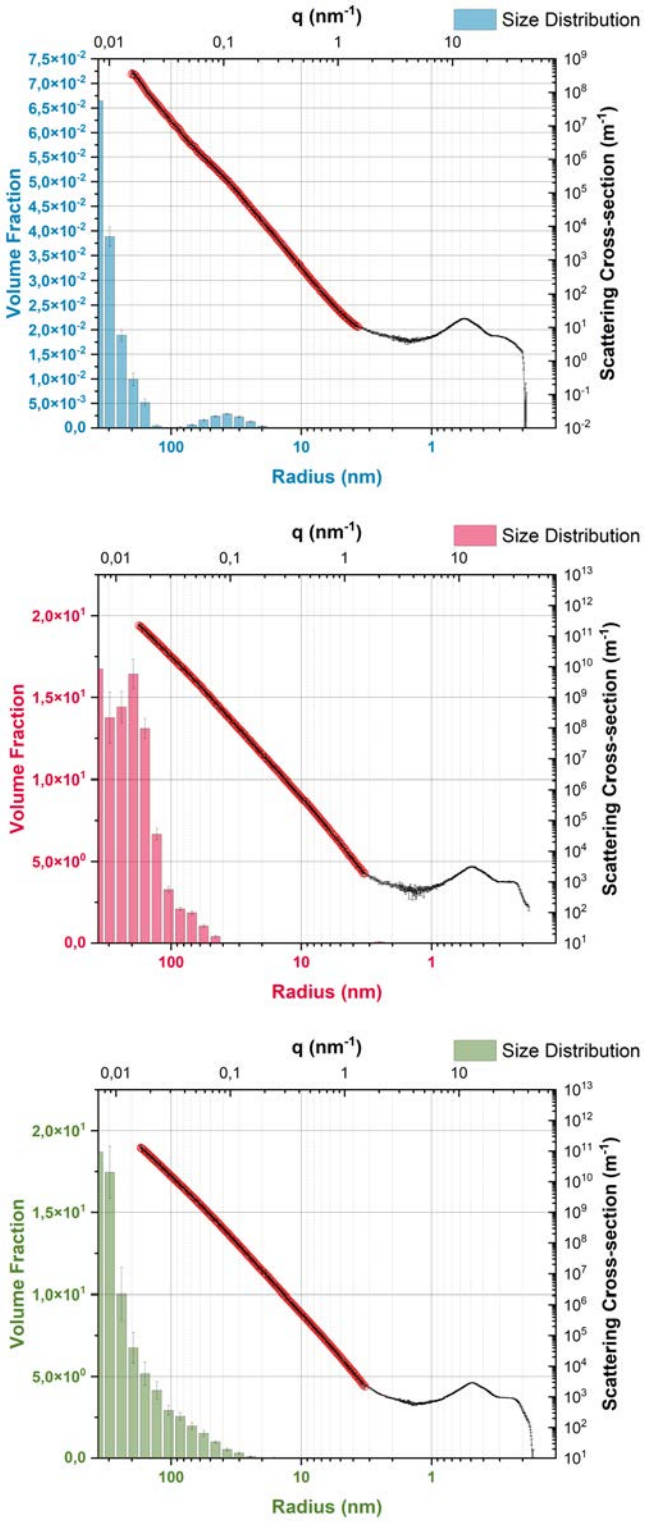


Figure 3.14: Results of the X-ray scattering experiments for nanoPP with increasing content of gold from the top (light blue = pure nanoPP) to red in the middle (0.1% gold) to the bottom (green = 0.5% gold). The results show the SAXS and WAXS measured with the MOUSE instrument [94]. The data (black) was curve-fitted (red line) in the SAXS range. The resulting size distributions are shown as radius-dependent histograms.

## 3.2 POLY(LACTIC ACID) NANOPLASTICS

The polyolefin nanoparticles presented in sections 3.1 represent particles prepared in a top-down method. Another possibility is to use a bottom-up method. This approach was used for the biopolymer poly(lactic acid) (PLA), which is increasingly used as a greener substitute for other plastics. Because of its rising popularity and its different solubility, PLA was chosen to use in the bottom-up method. Usually, when speaking of the synthesis of polymeric NPs in a bottom-up method, polymerisation of the monomers also takes place. The most common strategy for polymer NPs is (micro and mini) emulsion polymerisation [9, 29]. However, performing a complete polymerisation is not always feasible and the characterisation of the polymerisation products is not possible for all MNPs researchers. Therefore, the aim here is to show a way in which already characterised polymers with desired properties can be used to produce nanoplastics.
In our case, the polymer was purchased from a manufacturer and the polymer pellets were dissolved in an organic solvent, skipping the polymerisation. The solvent chosen was tetrahydrofuran (THF), which dissolves PLA as well as the non-ionic surfactant Pluronic F-127. Both of the solid polymers were dissolved completely in the first preparation step. Then, the solvent is exchanged from THF to water. The same volume of water is added to the THF solution. Under stirring, THF is evaporated, leaving a dispersion of PLA in water, stabilised with Pluronic F-127. In contrast to the top-down methods in Section 3.1, the upscale of the preparation is easier as well as the concentration of PLA in the dispersion is known since only the volatile organic solvent evaporates.
The resulting dispersion was analysed with the MALS instrument. Figure 3.15 (left) shows the hydrodynamic radii $R_h$ of three different batches, determined with a DLS instrument, in boxplots.

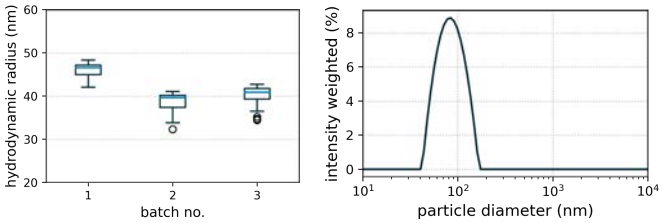


Figure 3.15: Results of DLS measurements. Left: boxplots of the hydrodynamic radii of three different batches of nanoPLA prepared in a bottom-up method; blue line: median hydrodynamic radius. Right: intensity-weighted size distribution of the nanoPLA with only a single maximum at 89 nm.

All three results show a relatively small size distribution, with radii ranging between 30 nm < $R_h$ < 50 nm. Because batch no. 3 was prepared on a larger scale, this batch was used for further analysis. Besides

the mean hydrodynamic radii of the particles, the size distribution and potentially larger aggregates were determined. The (intensity-weighted) size distribution in the range from 1 nm to 1000 nm as given in Figure 3.15 (right) shows only one narrow distribution with a maximum at 89 nm and no further distributions at larger sizes.

The single maximum makes this sample a fit candidate to use the MALS data to calculate the particle concentration in water, which can be performed with certain instruments. More detailed information on the process can be found in Section 2.3.1. Some modern instruments already offer the possibility to calculate the particle concentration as a feature of the instrument's software. Nonetheless, it is also of interest to perform these calculations with instruments, which yet do not offer these calculations as an instrument's feature, given they meet the conditions for these calculations i. e. multi-angle measurements.

The results of the MALS measurements are used to perform these calculations. Some other information on the material dispersed and the dispersion medium need to be known, too. To normalise the results of the normal MALS measurement, toluene, and solvent (in this case water) must also be measured. A first Python Notebook on the calculation of the particle concentration was published via GitHub [100]. The measurements used for this notebook were performed using an ALV 7004 MALS instrument (see Section 5.3). The implementation of the calculations was tested with a PS latex standard with a known concentration at different dilution levels.

The structure of the notebook can be summarised as follows. After importing the desired files of the DLS measurements for the sample, water (background) and toluene (reference), the density and the refractive index of the polymer type of the sample must be entered. After further computing, the notebook displays the intensity (here Count Rate (kHz)) of the three measurements over all measured angles. Here, noticeable differences can already be recognised. To calculate the concentration using Equation 2.9, an intensity-weighted particle size distribution is necessary. The notebook uses the CONTIN algorithm to determine this size distribution. The result of this calculation is output for all measurement angles and repetitions. Together with the differential scattering cross-section, which is calculated using the Mie theory Python module *miepython*, the particle concentration as a number and a mass concentration is calculated for all measuring angles and a median concentration is presented as a result. These results are shown in Table 3.7.

Comparing the results of the particle concentration calculated for the PLA dispersion with the PLA mass used in the synthesis, the values match quite well. However, there are different results for the calculated concentration depending on which toluene and water measurements are used. For the toluene and water measurements that were performed in 2021 before the laser was exchanged, the values

Table 3.7: Results of the particle concentration $c_{DLS}$ calculated with the Python Notebook [100] in comparison with the mass of PLA used in the synthesis. The median mass concentration and number concentration are listed for the use of two different sets of toluene (reference) and water (background) measurements, performed in 2021 and 2022

| Sample | $c$ (mg mL$^{-1}$) | $c_{DLS}$ (mg mL$^{-1}$) | $c_{DLS}$ (mL$^{-1}$) |
|---|---|---|---|
| PLA (2021) | $1.0 \pm 0.1$ | $0.8 \pm 0.5$ | $(4.5 \pm 2.5) \cdot 10^{12}$ |
| PLA (2022) | $1.0 \pm 0.1$ | $1.0 \pm 0.5$ | $(6.1 \pm 4.5) \cdot 10^{12}$ |

differ by 20%. If the same sample measurement (before the laser exchange) is used together with toluene and water measurements that were performed after the laser was exchanged in 2022, the values seem to falsely match exactly. This means that the reference and the background measurements are important for the result, even though their absolute scattering intensity is relatively low in comparison to the sample. The count rates of the sample and toluene and water before and after the laser exchange are compared in Figure 3.16

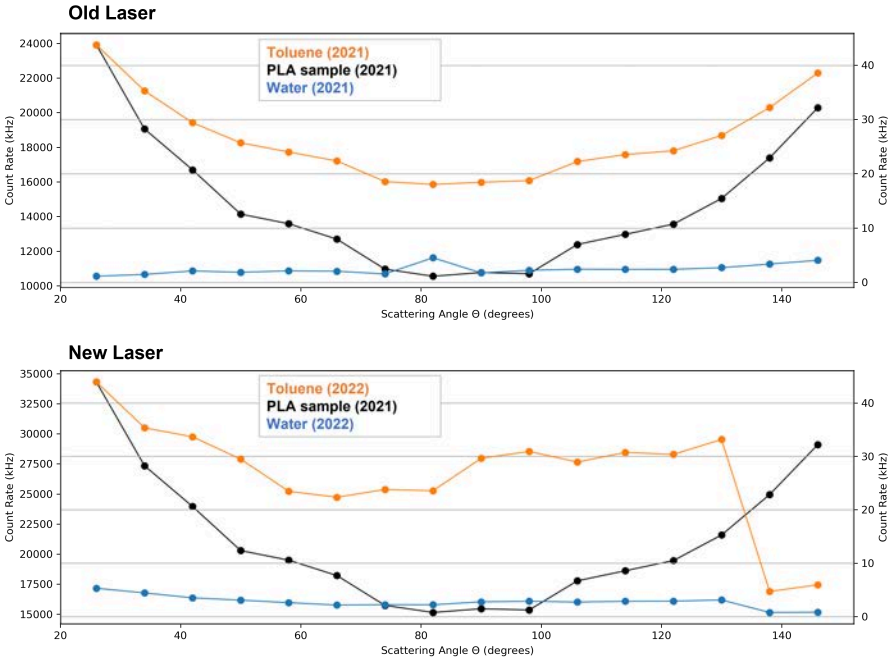


Figure 3.16: Count Rate of the DLS measurements of a PLA dispersion (black), toluene (orange) and water (blue) for all scattering angles. The measurements of toluene and water were performed before (upper graph) and after (lower graph) the exchange of the laser.

During the period of the study, the laser of the instrument had to be renewed, which also led to a new setup of the detectors etc. After

the exchange, the count rate for the detector at the highest scattering angles (one detector serves for two angles in the applied experimental setting), decreased drastically, especially for toluene. But the curve also differs slightly for the other angles. Additionally, the count rate of the PLA samples plotted in Figure 3.16 differs because the scaling factor measured for toluene with the new laser is different, leading to a minimum 30% higher count rate for the nanoPLA sample due to scaling. These differences show that close attention must be paid to which reference and background measurements are used for the calculation of the particle concentration in the device used. Rather, an order of magnitude of the particle concentration can be taken from the available notebook and not exact values. The geometry of the instrument setup can be changed so easily, which will lead to a big change in the scattering intensity and thus in the particle concentration, the application of the calculation for the very experimental instrument used here, might not be suitable for exact concentrations. An instrument, which is less influenced by the handling of the device, and fewer setup parts can be adapted by hand, is therefore prone to deliver more consistent results of the scattering intensity.

### 3.2.1 *Gold clusters for nanoplastic staining*

As mentioned before, metal-stained nanoplastics are usually produced by adding the metal particles in a bottom-up preparation method [87]. When nanoplastics are synthesised, it is essential, that the incorporated metal particles are small enough. Therefore, as part of the work on gold-containing nanoplastics, also the staining agent was synthesised, which could be used in a bottom-up approach used for the preparation of PLA nanoparticles. To have very small particles and not potentially increase the size of the stained nanoplastics, gold clusters were synthesised. Gold clusters possess unique optical and structural properties [101, 102] since they are even smaller ($\leq 1$ nm) than NPs ($1 - 100$ nm) and only consist of $2 - 1000$ atoms. To achieve this small size, the reaction, i. e. the particle growth, must be well controlled. The choice of the reaction conditions, such as the reducing agent and stabilising ligands (i. e. thiolate, selenoate, phosphine and acetylide) can lead to a certain size of the cluster [103–106]. However, no ionic liquid (IL) has been used for the synthesis of gold clusters. So far, ILs have only been used in the NPs synthesis [107] but their vast range of possible properties can make them also a suitable candidate for gold cluster synthesis. The advantage of the used IL 1-Ethyl-3-methylimidazolium dicyanamide ([Emim][DCA]) is, that it is the reducing agent for the gold salt $HAuCl_4 \cdot 3H_2O$ as well as the solvent of the gold clusters.

The preparation of the gold clusters is very simple. The gold salt is added to a vial containing the IL. The solution is stirred until all the salt is dissolved and then the vial is heated for 24 h at different

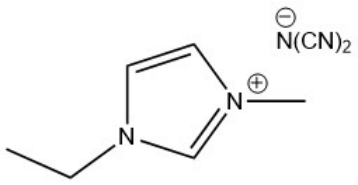


Figure 3.17: Stucture of the ionic liquid 1-Ethyl-3-methylimidazolium dicyanamide ([Emim][DCA]).

temperatures. The temperature was set to 20°C, 40°C, 60°C and 80°C, to compare the results. The initial light yellow colour of the mixtures changes with time depending on the temperature, ranging from light orange (80°C) to red (20°C), as shown in Figure 3.18.

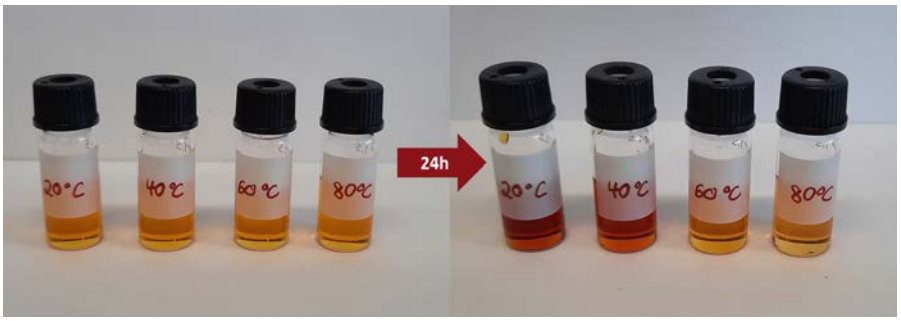


Figure 3.18: Vials with $HAuCl_4$ dissolved in [Emim][DCA]. Photographs were taken directly after dissolution (left) and after 24 h of reaction at 20, 40, 60 and 80°C (right). The yellow to light orange solution turns red (20°C), light red (40°C), orange (60°C) and light orange (80°C) in dependence of the reaction temperature.

The change of colour indicates the successful reduction from Au(III) salt to Au (0) particles. However, the colour is not the colour that can be observed for gold NPs. Because of the surface plasmon resonance, NPs show a dark red to purple colour depending on their size [21]. Therefore, the hypothesis is, that the IL reduces the $Au^{3+}$ into $Au^0$ atoms, which coalesce into clusters but are stabilised in the cluster form by the IL.

The samples shown in Figure 3.18, were measured with UV/Vis spectroscopy and are compared with the spectrum of the pure IL. The spectra are shown in Figure 3.19.

The IL [Emim][DCA] shows a strong absorption band with a maximum at a wavelength of 250 nm. This maximum equals an energy of 4.96 eV, which corresponds with the HOMO-LUMO gap of [Emim][DCA] reported in literature of $(4.77 \pm 0.53)$ eV [108]. The samples with the gold clusters show besides the absorption at wavelengths below 300 nm, that comes from the IL, additional absorption at wavelengths larger than 300 nm. Therefore, the spectrum of the IL was subtracted from the spectra of the clusters. The result is shown in the inset of Figure 3.19. The difference spectra show an intensive

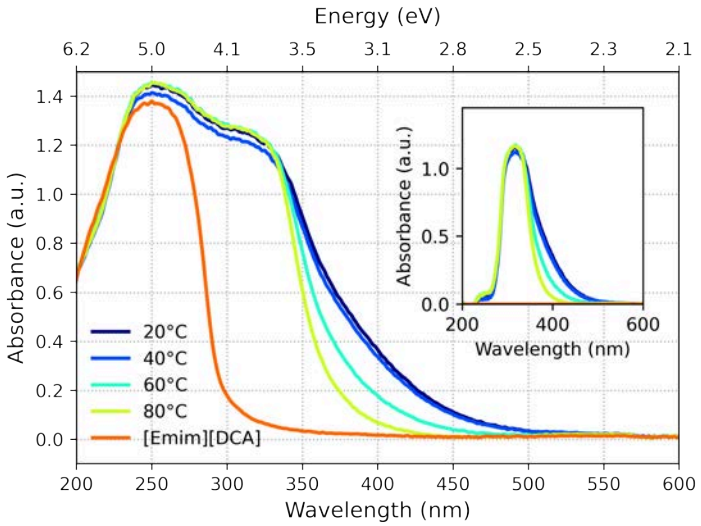


Figure 3.19: UV/Vis absorption spectra of the IL [Emim][DCA] and gold clusters in [Emim][DCA] synthesised at 20°C (a), 40°C (b), 60°C (c) and 80°C (d). Inset: Difference spectra after subtraction of the [Emim][DCA] spectrum.

absorption maximum at ca. 300 nm and a more or less pronounced shoulder towards higher wavelengths. The difference spectra were fitted with two Gaussian functions, that are added. The quantitative fit function is as follows

$$f(\lambda) = \sum_{i=1}^{2} \frac{a_i}{\sqrt{2\pi}\sigma_i} \exp^{-\frac{(\lambda-\lambda_i)^2}{2\sigma_i^2}} \tag{3.4}$$

with $a_i$ as the scaling factor, $\sigma_i$ the width and $\lambda_i$ the peak position. The resulting fits are shown in Figure 3.20 with the fit parameters given in Table 3.8.

Table 3.8: Curve fit parameters of the UV/Vis spectra of gold clusters at temperatures of $20 - 80$°C.

| $T$ (°C) | Peak maximum | | Peak width | | Absorbance | |
|---|---|---|---|---|---|---|
| | $\lambda_1$ (nm) | $\lambda_2$ (nm) | $\sigma_1$ (nm) | $\sigma_2$ (nm) | $f_1(\lambda_1)$ | $f_2(\lambda_2)$ |
| 20 | 312.0 | 354.0 | 32.4 | 55.1 | 0.83 | 0.45 |
| 40 | 312.3 | 353.7 | 32.0 | 54.5 | 0.81 | 0.42 |
| 60 | 316.2 | 401.2 | 33.5 | 26.5 | 1.20 | 0.10 |
| 80 | 314.7 | 398.7 | 29.7 | 13.9 | 1.22 | 0.03 |

A closer look at the curve fit parameters shows, that the first peak maximum $\lambda_1$ and the corresponding peak width $\sigma_1$ are very similar for all four samples. The second peak differs for the two samples synthesised at lower temperatures (20 and 40°C) and the samples synthesised at higher temperatures (60 and 80°C). The peak maximum $\lambda_2$

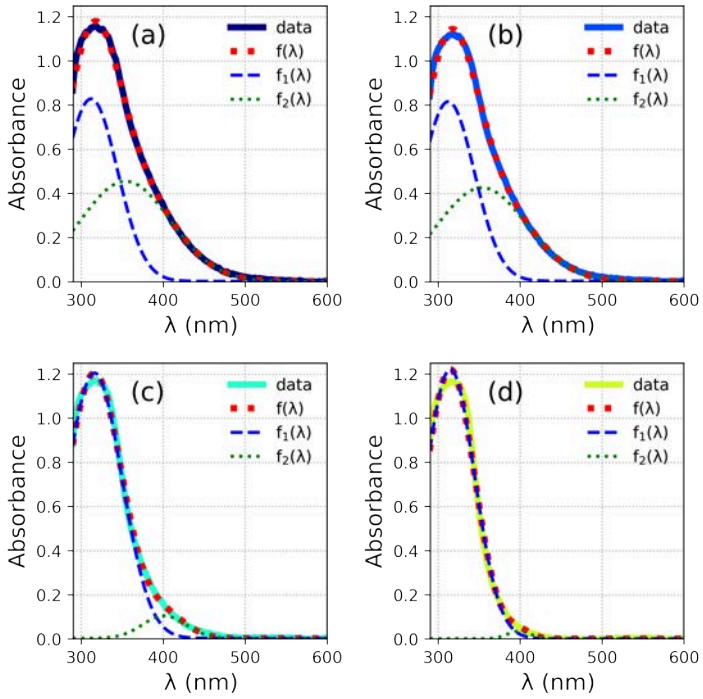


Figure 3.20: UV-Vis absorption difference spectra (solid lines) and curve fits $f(\lambda)$ using Equation 3.4 (red dotted lines) for clusters synthesized at 20°C (a), 40°C (b), 60°C (c) and 80°C (d). Contributions $f_1(\lambda)$ and $f_2(\lambda)$ are given (blue dashed and green dotted lines, respectively).

for the lower temperatures is ca. 45 nm lower than the peak maximum of the samples prepared at higher temperatures, while the peak width $\sigma_2$ is significantly lower. However, the significance of the second peak decreases for higher temperatures, because of the difference in the absorbance at the peak maxima $f(\lambda)$. While the ratio of $\frac{f_2(\lambda_2)}{f_1(\lambda_1)}$ is ca. 0.5 for the lower temperatures, it decreases to ca. 0.05 for higher temperatures. In literature, the optical properties of phosphine-protected gold clusters have been reported [109]. $Au_{20}$ clusters show a strong peak at 320 nm, which is linked to intraband transitions, while a peak at 419 nm is connected to interband transitions [109]. The peaks reported for $Au_{20}$ are therefore similar to the contributions found in the curve fit of the UV/Vis spectra.

The typical surface plasmon resonance of gold in the range of 520 to 540 nm which can be observed for gold nanoparticles of around 10 nm [110] cannot be observed for these samples. Because usually the gold nanoparticles with a diameter larger than 3 nm show the surface plasmon resonance [111]. SAXS and Matrix-assisted laser desorption/ionization time of flight mass spectrometry (MALDI-ToF MS) were performed to determine the size of the structures with more precise methods. The samples observed with these methods were also synthesised at temperatures of $20 - 80$°C.

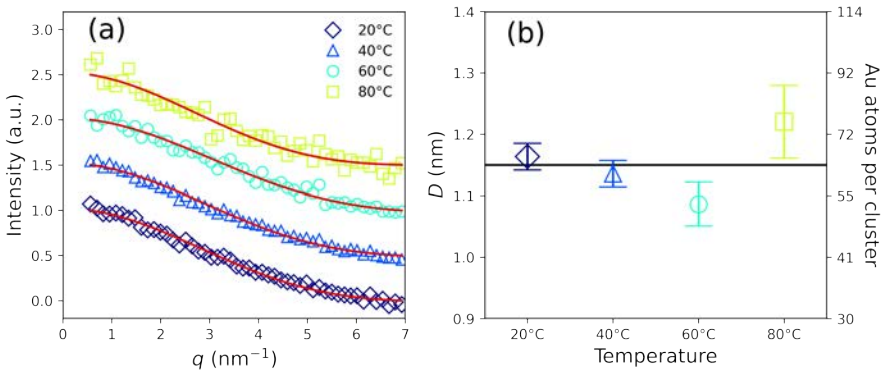


Figure 3.21: (a) SAXS data of clusters prepared at 20, 40, 60, and 80°C for 24 h (symbols) and curve fits using the simple sphere model (red solid lines). (b) The diameters of the clusters corresponding to the curve fits in panel (a). Error bars represent one standard deviation. The horizontal line represents the mean diameter of the samples of $D_{mean} = 1.15$ nm and 62 gold atoms per cluster. The right y-axis indicates the number of gold atoms per cluster.

The SAXS curves of the samples are shown in Figure 3.21 panel (a) and show the typical shape of particles with a tiny size. They were fitted using a spherical model [112]. The diameter of the particles synthesised at 20°C is $(1.16 \pm 0.03)$ nm, $(1.13 \pm 0.02)$ nm for 40°C, $(1.09 \pm 0.04)$ nm for 60°C and $(1.22 \pm 0.06)$ nm for 80°C. The resulting diameters of the clusters are plotted in Figure 3.21 panel (b) and assigned to the number of Au atoms per cluster. The number of atoms for the clusters determined with SAXS is $66 \pm 4$ (20°C), $61 \pm 4$ (40°C), $54 \pm 5$ (60°C), and $76 \pm 11$ (80°C), assuming a spherical shape and a volume of 0.0125 $nm^3$ for a gold atom.

With the number of gold atoms per cluster of 54 to 76 given by the SAXS analysis, the MALDI ToF MS results were expected to have a maximum peak at 10 638 m/z to 14 972 m/z for a neutral charge. However, numerous equidistant peaks are visible in the range of 1000 to 4000 m/z as shown in Figure 3.22 for all samples.

The peaks found in the spectra range from 5 gold atoms up to 18 gold atoms given a charge of z = 1. However, for all three samples gold clusters are present. The decreasing intensity of the peaks for higher m/z ratios indicates the fragmentation of the clusters during the measuring process. This could also be the reason for the difference in the number of gold atoms per cluster found in MALDI ToF MS and SAXS. It has been reported that an optimised experiment can prevent the sample from fragmentation [113]. For a further analysis of the exact size of the gold cluster by MALDI ToF MS, the preparation and experiment might be optimised to deliver better results. Nonetheless, the results indicate, that small gold structures were synthesised in the presented way. Further investigations on cluster formation kinetics are the subject of a publication that was submitted for publication [114].

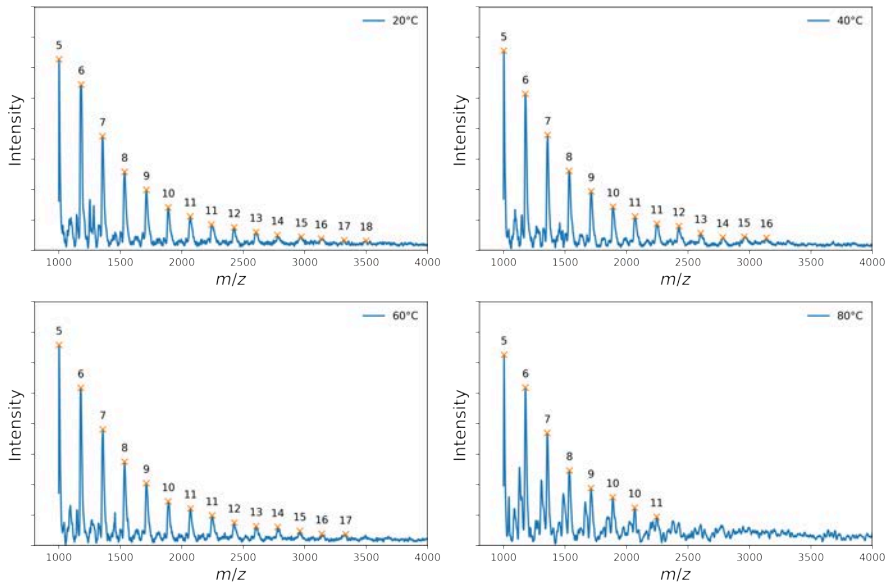


Figure 3.22: MALDI ToF MS spectra from samples of the IL containing gold clusters produced at temperatures of 20, 40, 60 and 80°C. Markers at the peaks denote the number of gold atoms corresponding to the m/z ratio of the peaks for z = 1.

Because the gold clusters proved to be small, they were used for the staining of bottom-up prepared PLA nanoplastics. Due to the IL as solvent, which does not evaporate, the gold clusters described here, were not used for staining the polyolefin nanoplastics in Section 3.1.4.

### 3.2.2 *Gold-containing nanoPLA*

The bottom-up method for nanoPLA synthesis was slightly adapted to combine the gold clusters with the PLA nanoplastics. After dissolving the polymer in the solvent THF, the gold cluster dispersion in the IL [Emim][DCA] was added to the polymer solution. Then the synthesis was completed in the usual way by adding Pluronic F-127 and water and finally removing the THF by heating. The resulting dispersion (shown in Figure 3.23) was again analysed with DLS. The dispersion is highly turbid and needs to be filtered and diluted to obtain a sample for measurements without multiple scattering.

The synthesis was performed for two different amounts of gold clusters. The results in Table 3.9 show, that an increase in the gold content leads to an increase in the particle size ($D_h$). The PDI of the PLA particles only increases slightly for the highest gold content. In total, the PDI of the dispersed particles is close to 0.1 which indicates a moderately disperse sample.

To check the optical properties of the nanoplastics, UV/Vis spectroscopy was performed. The spectra are shown in Figure 3.24. The dispersion of nanoPLA without gold does not show any absorption in


Figure 3.23: Photograph of the samples dispersed in water. Left: nanoPLA without gold. Middle: nanoPLA with 0.8% Au. Right: nanoPLA with 4.9% Au. All samples have a PLA concentration of $c_{\mathrm{PLA}} = 1.0 \cdot 10^{-3}$ g mL$^{-1}$.

Table 3.9: Hydrodynamic diameter $D_h$ and PDI of nanoPLA particles with different gold contents measured with DLS.

| Sample | $D_h$ (nm) | PDI |
|---|---|---|
| nanoPLA | $89.2 \pm 3.0$ | $0.11 \pm 0.02$ |
| nanoPLA + 0.8% Au | $198.0 \pm 10.8$ | $0.12 \pm 0.04$ |
| nanoPLA + 4.9% Au | $259.1 \pm 23.7$ | $0.18 \pm 0.03$ |

the range of $\lambda > 200$ nm, while the absorption of the pure gold clusters shows a broad and intense absorption band at wavelengths in the range $200 - 400$ nm as discussed before. The dispersion of nanoPLA with gold clusters added shows a combination of the two spectra. The absorbance is not as strong as it is for the pure gold clusters as the gold clusters are also more dilute in this sample. Nonetheless, the spectrum shows a broader absorption band in the range that can be observed for the gold clusters.

However, the results do not give sufficient information on the structure of the dispersion of nanoPLA with gold added. The UV/Vis absorption spectrum could also have these characteristics due to the mixture and dilution of the gold cluster dispersion. As an additional method, asymmetric flow field flow fractionation ($AF_4$) was used to see if two different populations i. e. a separation of nanoPLA and gold clusters occurs. The fractograms of the $AF_4$ experiment (Figure 3.25) show only a single population for the nanoPLA samples which contain gold clusters. The UV detector is of special interest here, because the clusters show a strong absorption here. Besides the void peak at a time of ca. 18 min, no additional populations are detected. Furthermore,

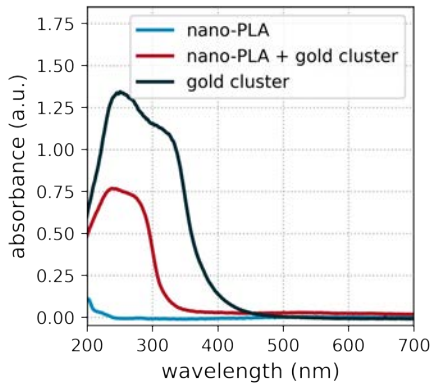


Figure 3.24: UV/Vis absorption spectra of a nanoPLA dispersion (light blue), a nanoPLA dispersion with gold clusters added during synthesis (red) and the pure gold cluster dispersion (black).

the results of the $AF_4$ support the finding of a larger diameter for the additional gold content done with DLS. The fractograms of the nanoPLA without gold and the nanoPLA with gold content differ significantly in the time they were detected, indicating that the nanoPLA particles are much smaller than the nanoPLA + Au.

To gain more information on the samples and their structure, the samples were examined with transmission electron microscopy (TEM). The samples were filtered with a syringe filter (450 nm PTFE membrane) before applying them onto a TEM grid. Unfortunately, the pure nanoPLA samples (**??**) did not have sufficient contrast, especially in comparison to their small size. The nanoPLA particles appear as dark spots without sharp delimitations. Therefore, the micrographs for the nanoPLA samples were not evaluable.

However, the TEM images of the nanoPLA sample with gold look different (**??**). Here, only the sample with a lower gold content was examined, because the higher concentration of IL was interfering with the drying process of the samples onto the TEM grid and deteriorated the quality of the recordings. The particles appear as light spheres surrounded by dark clouds of higher contrast. A closer look at the two single particles shows, that the high-contrast substance, i. e. the gold clusters, accumulates at the surface of the sphere.

With their lighter core and darker shell, the particles seem to be hollow. This kind of capsular structure was reported for PLGA (poly(lactic-co-glycolic acid)) nanoparticles before [115]. This indicates that the addition of the gold clusters dispersed in the IL presumably leads to the formation of a hollow structure. However, electron microscopy was difficult to perform for the nanoPLA samples with gold clusters, too. One reason is the very small size of the gold clusters, which decreases the contrast of the particles, even though they have a high atomic number in contrast to the organic PLA and other polymer

types. Therefore, the use of the prepared gold clusters is not suitable for the staining of nanoplastics, when it comes to electron microscopy.

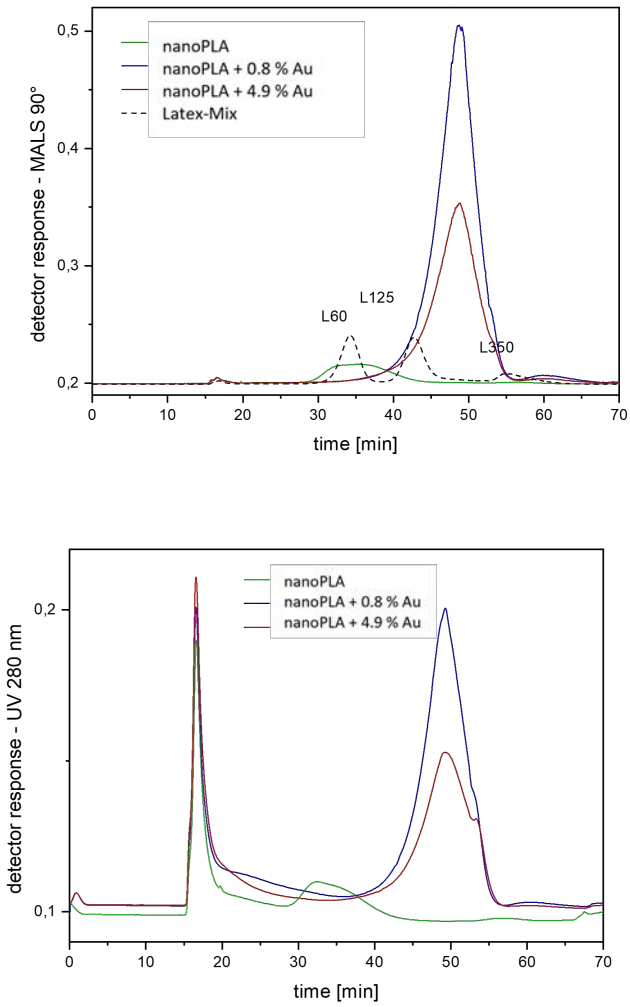


Figure 3.25: Resulting fractograms of the $AF_4$ experiments for nanoPLA (green), nanoPLA + 0.8% Au (blue) and nanoPLA + 4.9% Au (red). Top: Light scattering (90°) detector response in comparison to the mixture of three different latex standards. Bottom: UV (280 nm) detector response.

# 4

# CONCLUSION AND OUTLOOK

The method presented in this work for the preparation of nanoplastic dispersions by mechanical stress is characterised by good repeatability and stability due to the strongly negative zeta potential. Furthermore, the particle size and concentration can be adjusted by modifying the preparation parameters. The dispersions can also be easily characterised with DLS instruments, which can be found in many laboratories, which makes quality controls easily available for users.

Since the method could be applied to both PP and PE, it is conceivable that, with a slight adjustment of the parameters, similar results can also be obtained with other polyolefins or similar polymer types. Preliminary experiments for poly(ethylene terephthalate) (PET) with a slightly modified preparation method also showed the formation of nanoplastic particles. Likewise, the results showed that nanoplastic particles can also be easily produced from PP of other molar mass or even with additives (gold in this case). Therefore, these reference materials will certainly not remain the only ones and there is an opportunity to produce suitable nanoplastic reference materials for specific purposes that have the desired molar mass or additives. The interest in such nanoplastic reference materials is very high in the field of microplastic and nanoplastic research, since only a few such materials are available, so even before the official certification as reference materials, samples have been requested by several other European research institutes to use them in their own research.

Own preliminary tests of the interaction with pollutants such as lead salts ($PbCl_2$), indicated an attractive interaction of nanoplastic particles and $Pb^{2+}$ ions. This could possibly pose harm as the plastic particles could act as a carrier for the pollutants into the human body. However, further tests need to be carried out.

In the second part of this thesis, the synthesis of PLA nanoplastic dispersions with a bottom-up method seems an easy-to-scale-up way to produce these nanoplastic particles. However, combining these PLA particles with gold clusters proved not to be as promising as thought, because, they lead to a different structure of the loaded particles. Furthermore, the very small size of the gold clusters was complicating the detectability in (transmission electron) microscopy. Tests for different staining materials for the PLA nanoplastics could help to improve the detectability.

However, the detection and characterisation of the prepared nanoplastics remain challenging, even though they are only dispersed in water at higher concentrations and not in environmental matrices. Hopefully,

nanoplastic particles prepared with the method described in this thesis can help to improve detection and characterisation methods.

# 5

# EXPERIMENTAL

## 5.1 MATERIAL

All chemicals were used as received without further purification. Polypropylene (isotactic, average $\bar{M}_w \sim 12000\ \mathrm{g\,mol^{-1}}$, average $\bar{M}_n \sim 5000\ \mathrm{g\,mol^{-1}}$ and isotactic, average $\bar{M}_w \sim 250000\ \mathrm{g\,mol^{-1}}$, average $\bar{M}_n \sim 67000\ \mathrm{g\,mol^{-1}}$) and Polyethylene (average $\bar{M}_w \sim 4000\ \mathrm{g\,mol^{-1}}$, average $\bar{M}_n \sim 1700\ \mathrm{g\,mol^{-1}}$) were purchased from Sigma Aldrich. Acetone (p.A., min. 99.5%, ChemSolute) was purchased from Th.Geyer. The water for the preparation was purified using a Sartorius arium 611DI purifier. Folded filters of grade 2105 (fast filtering, particle retention $12 - 15\ \mu\mathrm{m}$, by LabSolute) were purchased from Th.Geyer. Ingeo Biopolymer 2003D (Polylactic acid) was purchased from NatureWorks. Tetrachloroauric (III) acid trihydrate ($HAuCl_4 \cdot 3\ H_2O$) was obtained from Sigma Aldrich ($\geq$ 99.9%). 1-Ethyl-3-methylimidazolium dicyanamide ([Emim][DCA], $>$ 98%) was purchased from Iolitec Ionic Liquids Technologies GmbH.

## 5.2 PREPARATION

*Polyolefin nanoplastics*

The polyolefin nanoparticles dispersed in water were prepared with different amounts of pristine polymer and different mechanical stress durations. A more detailed discussion of the preparation parameters and their influence on the nature of the products can be found in section 3.1. In the following paragraph, the preparation of the reference material candidates is presented as a representative of all polyolefin nanoparticle preparations carried out.

The polymer (6 g PP pellets or PE powder) was placed in a high-walled 400 mL beaker. 115 mL acetone was added to the beaker. The beaker was cooled using a water and ice bath. Then the polymer was processed using a T18 digital Ultra-Turrax® disperser (IKA GmbH Staufen, Germany) at a speed of 18 000 rpm for 10 minutes. After the processing, the disperser tool was cleaned with 5 mL of additional acetone to remove plastic debris. The dispersion in acetone was filtered to remove bigger plastic debris. For exchanging the solvent from acetone to water, acetone was evaporated to a volume of ca. 30 mL. Then 115 mL of purified water was added to the dispersion. The liquid turns turbid immediately. The remaining acetone was evaporated and

the dispersion was filtered again to remove aggregates formed during the evaporation process. The resulting dispersion can be analysed using DLS and ELS.

*Reference Material*

The preparation of the nanoplastic dispersions was repeated for ca. 60 times. All of the batches of nanoplastic dispersions, that passed the z-score tests (see Section 3.1) in all three categories were added to a 5 L bottle. The bottle was equipped with a seripettor bottle top dispenser (BRAND GmbH & Co. KG, Wertheim, Germany) with a 10 mL dispensing volume. The bottle was swirled to maintain a homogeneous mixture of the dispersion. Then 10 mL screw top glass bottles were filled with the dispersion. After every $15^{\text{th}}$ aliquot bottle was filled, the stock bottle was swirled again. Finally, the small bottles were heated to 90°C for 2 h, to pasteurise the samples. Further tests were carried out with the pasteurised samples.

*Gravimetric determination of the polymer concentration*

To prevent the loss of sample, the gravimetric analysis was performed in an open aluminium sample pan (designed for DSC measurements). Each sample pan used was weighted empty. Then, it was heated to 150°C on a hot plate and a 1 mL aliquot of the sample was added to the sample pan dropwise. Care was taken to ensure that all of the sample volume was added to the pan and not spilt. Eventually, the pan was heated for an additional 15 min to ensure the complete evaporation of the solvent. The sample pan was weighted again and the weight difference was calculated. For each dispersion, this determination was performed three times.

*Gold-stained polypropylene*

10 g of PP pellets (average $\bar{M}_w \sim 12000\ \mathrm{g\,mol^{-1}}$, average $\bar{M}_n \sim 5000\ \mathrm{g\,mol^{-1}}$) was heated in a beaker to 170°C. To homogenise the melt, it was stirred with a glass stirring rod. When all pellets were melted, 0.02 g and 0.1 g tetrachloroauric (III) acid trihydrate ($HAuCl_4 \cdot 3\ H_2O$, $c(\mathrm{Au})_{\mathrm{final}} = 0.1\%$ and 0.5% (m/m) respectively) was added to the melt. The clear polymer turned brown. When all gold was homogeneously mixed within the polymer melt, the melt was poured onto a heat-resistant glass plate. The polymer solidified again quickly. The solid polymer was slightly crushed to use it for further investigations.

*Poly(lactic acid) nanoparticles*

In these experiments, granular Polylactide (PLA) with a molar mass of $\bar{M}_n \sim$ 98000 g mol$^{-1}$(Đ = 2.11) was used.

*Bottom-up synthesis of nanoPLA*

50 mg of granular PLA together with 150 mg (0.3 wt%) Pluronic F-127 were dissolved in 50 mL tetrahydrofuran (THF). Afterwards, 50 mL of water was added under stirring. The THF was completely evaporated under stirring at a temperature of 50°C.

*Bottom-up synthesis in combination with gold clusters*

50 mg of granular PLA together were dissolved in 50 mL tetrahydrofuran (THF). 0.4 mL of a solution of gold clusters in 1-ethyl-3-methylimidazolium dicyanamide ([Emim][DCA]) was added and dispersed in THF under stirring. Then, 150 mg (0.3 wt%) Pluronic F-127 were added. Afterwards, 50 mL of water was added and THF was evaporated completely at a temperature of 50°C.
The success of the reaction and the presence of gold clusters was determined with UV-Vis spectroscopy.

*Synthesis of gold clusters*

16 mg of tetrachloroauric (III) acid trihydrate ($HAuCl_4 \cdot 3\ H_2O$) was added to 1 mL of 1-ethyl-3-methyl-imidazolium dicyanamide ([Emim][DCA]) in a screw-top bottle ($c_{Au} = 8$ mg mL$^{-1}$). The gold salt was dissolved via stirring at room temperature. After the complete dissolution, the bottle was stored for 24 hours at the respective temperature. The synthesis was carried out at $20, 40, 60$ and 80°C. For temperatures of $40 - 80$°C, an appropriately pre-tempered drying oven was used. To obtain the UV-Vis measurement series, small amounts of samples were taken and measured at the respective time during the synthesis. These aliquots were then discarded. For the SAXS measurement series, the samples were inserted into the instrument after dissolving the salt and the sample holder was heated to the desired temperature so that the reaction could be observed directly.

## 5.3 METHODS

*Asymmetric flow field flow fractionation (AF4)*

The fractionation was performed using an AF 2000 A4F system (Postnova Analytics GmbH, Landsberg, Germany) with a refractive index (RI) detector, a UV detector ($\lambda = 280$ nm) and a multi-angle light scattering (MALS) detector. A 10 kDa RC membrane was used together with double distilled water (filtrated 0.1 mm; with added $NaN_3$ (200 mg $L^{-1}$). The calibration was carried out with a mixture of latex standards with geometric diameters of 60, 125, and 350 nm.

*Dynamic light scattering (DLS) and Electrophoretic light scattering (ELS)*

The measurements were performed with different instruments. Firstly, multiangle light scattering measurements were performed using an ALV 7004 device with a He-Ne-Laser ($\lambda = 632.8$ nm) from ALV (Laser Vertriebs GmbH, Langen Germany). A Millex 0.45 µm PVDF syringe filter was used for filtering the samples. The glass cuvettes used were cleaned with acetone before filling them with the sample. Measurements were performed at scattering angles of $2\theta = 26^\circ - 146^\circ$ in $8^\circ$ steps and at a temperature of $20 \pm 1$°C. Three measurements, lasting 30 s each, were carried out at each angle.

Secondly, measurements of $D_h$, PDI and $\zeta$ potential for the homogeneity and stability studies were performed with a Zetasizer Nano instrument (Malvern Panalytical Ltd., Worcestershire, UK) working in backscattering geometry at an angle of $2\theta = 173^\circ$. The z-score studies of the batches and the homogeneity and stability studies of the reference material candidates were performed on this instrument using a DTS1070 cell for $\zeta$ potential measurements. For the titration experiment, the Zetasizer was equipped with an MPT-2 titrator & degasser (Malvern Panalytical Ltd.). The titrant reservoir of the titrator was equipped with two different concentrations of HCl solution ($c_1 = 0.25$ M and $c_2 = 0.01$ M). A pH range from 7 towards lower pH values of ca. 2 was covered with the automated titration.

Additionally, the samples were measured with an Anton Paar LiteSizer 500 (Anton Paar GmbH, Graz, Austria). This instrument combines the multiangle measurement and the $\zeta$ potential measurement. The detectors are positioned at fixed angles ($15^\circ, 90^\circ and 175\circ$). The measurement in vertical scattering at $90^\circ$ is not possible for ELS measurements due to the geometry of the omega cuvette.

*Electron microscopy (EM)*

SED was performed with a Zeiss Supra 40 Scanning Electron Microscope (Zeiss, Oberkochen, Germany), at 10 kV acceleration voltage,

4.8 mm WD, in SE InLens mode, and at different magnifications. Before measurement, the flask with the nanoPP dispersion was carefully shaken. 3 µL of the suspension (PP, ID336) were drop-casted on the carbon tape and allowed to dry for ca. 24 h under normal laboratory conditions.

The transmission electron microscope JEM-1011 (JEOL GmbH) at an acceleration voltage of 80 kV was used to perform the TEM investigations. The nanoPLA samples were filtered with a PTFE syringe filter (pore size = 450 nm) prior to dropping them on carbon-coated copper grids and rapidly drying by removing the excess liquid with filter paper.

*Gel permeation chromatography (GPC) / Size-exclusion chromatography (SEC)*

This analytical method describes the determination of the molar masses and molar mass distribution of polyolefins after gel chromatographic separation on GPC columns (3× PSS POLYOLEFIN linear XL, 30 × 0.8 cm, 10µm pore size). This method was a relative method. The molar masses were calculated based on a universal calibration with 12 polystyrene standards (Polymer Standards Service GmbH), over the range of $M_p = 1.2 \cdot 10^7 - 266$ g mol$^{-1}$ by conversion according to Mark–Houwink parameters. A high-temperature GPC equipped with infrared (IR4) and viscosity detection (PolymerChar GPC IR), an isocratic HPLC pump (PSS-Security), and an autosampler (PolymerChar GPC-IR) running at 160°C were used. The eluent used was 1,2,4-trichlorobenzene stabilized with 0.1% BHT. The flow rate was 1.0 mL min$^{-1}$. Injection of 200 µL of an approximately 2 mg mL$^{-1}$(8 mL total) solution in the eluent (internal filtration unit) then followed. The error range was estimated at approximately ±10%.

*Matrix-assisted laser desorption/ionization time of flight mass spectrometry (MALDI-TOF MS)*

An Autoflex maX (Bruker Daltonik GmbH, Bremen Germany) was used. The gold cluster samples were used as prepared and dropped (1µL) on a stainless steel target. After drying, the sample holder was inserted and samples were irradiated with a Ny-YAG Smartbeam laser working at 355 nm and 1000 Hz. Typically, 1000 laser shots from 4 different places of the spot were accumulated to a spectrum. Calibration was done using peptide standards (Bruker). FlexControl and FlexAnalysis (Bruker) were used for recording and calculating raw data.

*Small-angle X-ray scattering (SAXS)*

Small-angle X-ray scattering (SAXS) measurements were performed in a polycarbonate flowthrough capillary at 21(1) °C with a SAXSess camera (Anton Paar, Graz, Austria). This camera was attached to a laboratory X-ray generator (PW3830, PANalytical) and operated with a fine-focus glass X-ray tube at a voltage of 40 kV and a current of 40 mA (Cu $K_\alpha, \lambda = 0.1542$ nm). A focusing multilayer optics and a block collimator provided a monochromatic primary beam with low background noise.

In addition to the SAXSess device, the MOUSE instrument [94] was used for SAXS and wide-angle X-ray scattering (WAXS). X-rays were generated from a microfocus X-ray tube, followed by multilayer optics to monochromise the X-ray beam at a wavelength of $\lambda = 0.154$ nm (Cu $K_\alpha$). Three sets of scatterless slits are used to collimate the beam before the sample. The scattered radiation is collected on an in-vacuum Dectris Eiger R 1M detector, mounted on a three-axis motorized platform placed at distances ranging from $138 - 2508$ mm from the sample. Solid samples were mounted in the beam between two pieces of scotch magic tape. The resulting data were subsequently processed to absolute intensity using the DAWN software package and standardised procedures [116, 117]. Sample thicknesses were derived using calculated sample absorption coefficients, derived from estimates of the sample compositions and gravimetric densities. SAXS data analysis was performed using the McSAS software package, to obtain "form-free" size distributions using Monte Carlo methods [118].

*Ultraviolet-visible spectroscopy (UV/Vis)*

UV-Vis measurements were performed using a BLACK-Comet C-50 Spectrometer (StellarNet Inc., Florida, USA) with an SL5 Deuterium + Halogen Light Source (StellarNet Inc.). A demountable quartz cuvette (QS, Hellma GmbH & Co. KG, Müllheim, Germany) with a 0.10 mm light path was used. The measurements were integrated over a period of 50 ms and averaged for 5 cycles.

# BIBLIOGRAPHY


[1] H. Staudinger. "Über Polymerisation." In: *Berichte der deutschen chemischen Gesellschaft (A and B Series)* 53.6 (1920), pp. 1073–1085.

[2] Rolf Mülhaupt. "Hermann Staudinger and the Origin of Macromolecular Chemistry." In: *Angewandte Chemie International Edition* 43.9 (Feb. 20, 2004), pp. 1054–1063. DOI: 10.1002/anie.200330070.

[3] Karl Ziegler. "Das Mülheimer Normaldruck-Polyäthylen-Verfahren." In: *Angew. Chem.* 67.19 (Oct. 7, 1955). In collab. with E. Holzkamp, H. Breil, and H. Martin, pp. 541–547.

[4] G. Natta. "Stereospezifische Katalysen und isotaktische Polymere." In: *Angewandte Chemie* 68.12 (June 21, 1956), pp. 393–403. DOI: 10.1002/ange.19560681202.

[5] Roland Geyer, Jenna R. Jambeck, and Kara Lavender Law. "Production, use, and fate of all plastics ever made." In: *Science Advances* 3.7 (2017), e1700782. DOI: 10.1126/sciadv.1700782.

[6] Richard C. Thompson, Ylva Olsen, Richard P. Mitchell, Anthony Davis, Steven J. Rowland, Anthony W. G. John, Daniel McGonigle, and Andrea E. Russell. "Lost at Sea: Where Is All the Plastic?" In: *Science* 304.5672 (May 7, 2004), pp. 838–838. DOI: 10.1126/science.1094559.

[7] Stephanie Reynaud, Antoine Aynard, Bruno Grassl, and Julien Gigault. "Nanoplastics: From model materials to colloidal fate." In: *Current Opinion in Colloid & Interface Science* 57 (Feb. 1, 2022), p. 101528. DOI: 10.1016/j.cocis.2021.101528.

[8] Joanna M. Gonçalves and Maria João Bebianno. "Nanoplastics impact on marine biota: A review." In: *Environmental Pollution* 273 (Mar. 15, 2021), p. 116426. DOI: 10.1016/j.envpol.2021.116426.

[9] Katharina Landfester, Nina Bechthold, Franca Tiarks, and Markus Antonietti. "Formulation and Stability Mechanisms of Polymerizable Miniemulsions." In: *Macromolecules* 32.16 (Aug. 1, 1999), pp. 5222–5228. DOI: 10.1021/ma990299+.

[10] C Rouzes, M Leonard, A Durand, and E Dellacherie. "Influence of polymeric surfactants on the properties of drug-loaded PLA nanospheres." In: *Colloids and Surfaces B: Biointerfaces* 32.2 (Oct. 15, 2003), pp. 125–135. DOI: 10.1016/S0927-7765(03)00152-8.

[11] International Organization for Standardization. *ISO/TS 80004-1:2015 Nanotechnologies - Vocabulary*. 2015.

[12] Ian Freestone, Nigel Meeks, Margaret Sax, and Catherine Higgitt. "The Lycurgus Cup — A Roman nanotechnology." In: *Gold Bulletin* 40.4 (Dec. 1, 2007), pp. 270–277. DOI: 10.1007/BF03215599.

[13] W. J. Stark, P. R. Stoessel, W. Wohlleben, and A. Hafner. "Industrial applications of nanoparticles." In: *Chem. Soc. Rev.* 44.16 (2015), pp. 5793–5805. DOI: 10.1039/C4CS00362D.

[14] Franklin Tao and James Spivey. *Metal Nanoparticles for Catalysis*. Catalysis Series. The Royal Society of Chemistry, 2014. P001. ISBN: 978-1-78262-033-4.

[15] Andrew N. Shipway, Eugenii Katz, and Itamar Willner. "Nanoparticle Arrays on Surfaces for Electronic, Optical, and Sensor Applications." In: *ChemPhysChem* 1.1 (Aug. 4, 2000), pp. 18–52. DOI: 10.1002/1439-7641(20000804)1:1<18::AID-CPHC18>3.0.CO;2-L.

[16] Laxmidhar Nayak, Smita Mohanty, Sanjay Kumar Nayak, and Ananthakumar Ramadoss. "A review on inkjet printing of nanoparticle inks for flexible electronics." In: *J. Mater. Chem. C* 7.29 (2019), pp. 8771–8795. DOI: 10.1039/C9TC01630A.

[17] de Jong. "Drug delivery and nanoparticles: Applications and hazards." In: *IJN* (June 2008), p. 133. DOI: 10.2147/IJN.S596.

[18] Maqusood Ahamed, Mohamad S. AlSalhi, and M.K.J. Siddiqui. "Silver nanoparticle applications and human health." In: *Clinica Chimica Acta* 411.23 (Dec. 14, 2010), pp. 1841–1848. DOI: 10.1016/j.cca.2010.08.016.

[19] K. Ted Thurn, Eric M. B. Brown, Aiguo Wu, Stefan Vogt, Barry Lai, Jörg Maser, Tatjana Paunesku, and Gayle E. Woloschak. "Nanoparticles for Applications in Cellular Imaging." In: *Nanoscale Research Letters* 2.9 (Aug. 15, 2007), p. 430. DOI: 10.1007/s11671-007-9081-5.

[20] Vincenzo Amendola, Roberto Pilot, Marco Frasconi, Onofrio M Maragò, and Maria Antonia Iatì. "Surface plasmon resonance in gold nanoparticles: a review." In: *J. Phys.: Condens. Matter* 29.20 (May 24, 2017), p. 203002. DOI: 10.1088/1361-648X/aa60f3.

[21] Nardine S. Abadeer and Catherine J. Murphy. "Recent Progress in Cancer Thermal Therapy Using Gold Nanoparticles." In: *J. Phys. Chem. C* 120.9 (Mar. 10, 2016), pp. 4691–4716. DOI: 10.1021/acs.jpcc.5b11232.

[22] Hans C Fischer and Warren CW Chan. "Nanotoxicity: the growing need for in vivo study." In: *Current Opinion in Biotechnology* 18.6 (Dec. 1, 2007), pp. 565–571. DOI: 10.1016/j.copbio.2007.11.008.

[23] Giyaullah Habibullah, Jitka Viktorova, and Tomas Ruml. "Current Strategies for Noble Metal Nanoparticle Synthesis." In: *Nanoscale Research Letters* 16.1 (Mar. 15, 2021), p. 47. DOI: 10.1186/s11671-021-03480-8.

[24] Patrick E. J. Saloga and Andreas F. Thünemann. "Microwave-Assisted Synthesis of Ultrasmall Zinc Oxide Nanoparticles." In: *Langmuir* 35.38 (Sept. 24, 2019), pp. 12469–12482. DOI: 10.1021/acs.langmuir.9b01921.

[25] Malín G. Lüdicke, Jana Hildebrandt, Christoph Schindler, Ralph A. Sperling, and Michael Maskos. "Automated Quantum Dots Purification via Solid Phase Extraction." In: *Nanomaterials* 12.12 (2022). DOI: 10.3390/nano12121983.

[26] C. Schindler and R.A. Sperling. "Process Control for the Continuous Synthesis of Quantum Dots via Inline Process Analytics." In: *Chemie Ingenieur Technik* 88.9 (Sept. 1, 2016), pp. 1224–1225. DOI: 10.1002/cite.201650319.

[27] Chow Pei Yong and Leong Ming Gan. "Microemulsion Polymerizations and Reactions." In: *Polymer Particles: -/-*. Ed. by Masayoshi Okubo. Berlin, Heidelberg: Springer Berlin Heidelberg, 2005, pp. 257–298. ISBN: 978-3-540-31565-0.

[28] Katharina Landfester, F.Joseph Schork, and Victor A Kusuma. "Particle size distribution in mini-emulsion polymerization." In: *Comptes Rendus Chimie* 6.11 (Nov. 1, 2003), pp. 1337–1342. DOI: 10.1016/j.crci.2003.07.019.

[29] Katharina Landfester, Nina Bechthold, Stephan Förster, and Markus Antonietti. "Evidence for the preservation of the particle identity in miniemulsion polymerization." In: *Macromolecular Rapid Communications* 20.2 (Feb. 1, 1999), pp. 81–84. DOI: 10.1002/(SICI)1521-3927(19990201)20:2<81::AID-MARC81>3.0.CO;2-G.

[30] Peter W. Atkins, Julio de Paula, and James J. Keeler. *Atkins' physical chemistry*. 11th. Oxford: Oxford University Press, 2018. 908 pp. ISBN: 978-0-19-876986-6.

[31] Mark J. Kirwan, Sarah Plant, and John W. Strawbridge. "Plastics in Food Packaging." In: *Food and Beverage Packaging Technology*. Apr. 1, 2011, pp. 157–212. ISBN: 978-1-4443-9218-0.

[32] PlasticsEurope AISBL. *Plastics - Architects of modern and sustainable buildings*. 2012. URL: https://plasticseurope.org/wp-content/uploads/2021/10/Final_BC_brochure_111212_web_version_UPD2018.pdf (visited on 10/04/2022).

[33] Irving Skeist. *Handbook of adhesives*. Springer Science & Business Media, 2012. ISBN: 1-4613-0671-X.

[34] Ana Šaravanja, Tanja Pušić, and Tihana Dekanić. "Microplastics in Wastewater by Washing Polyester Fabrics." In: *Materials* 15.7 (2022). DOI: 10.3390/ma15072683.

[35] Chrysanthos Maraveas. "Environmental Sustainability of Plastic in Agriculture." In: *Agriculture* 10.8 (2020). DOI: 10.3390/agriculture10080310.

[36] Alireza Aminoroaya, Rasoul Esmaeely Neisiany, Saied Nouri Khorasani, Parisa Panahi, Oisik Das, and Seeram Ramakrishna. "A Review of Dental Composites: Methods of Characterizations." In: *ACS Biomater. Sci. Eng.* 6.7 (July 13, 2020), pp. 3713–3744. DOI: 10.1021/acsbiomaterials.0c00051.

[37] Kalpana S. Katti. "Biomaterials in total joint replacement." In: *Colloids and Surfaces B: Biointerfaces* 39.3 (Dec. 10, 2004), pp. 133–142. DOI: 10.1016/j.colsurfb.2003.12.002.

[38] Duales System Deutschland GmbH. *Der Grüne Punkt und das Duale System - Einfach erklärt*. June 2016. URL: https://www.gruener-punkt.de/fileadmin/Dateien/Downloads/PDFs/mediathek/gruener-punkt-infoflyer_einzelseiten.pdf.

[39] The Plastic Soup Foundation. *The Plastic Soup Foundation*. URL: https://www.plasticsoupfoundation.org/en/.

[40] The Ocean Cleanup. *The Ocean Cleanup*. URL: https://theoceancleanup.com/.

[41] Ghada Atiwesh, Abanoub Mikhael, Christopher C. Parrish, Joseph Banoub, and Tuyet-Anh T. Le. "Environmental impact of bioplastic use: A review." In: *Heliyon* 7.9 (Sept. 1, 2021), e07918. DOI: 10.1016/j.heliyon.2021.e07918.

[42] Giulia Fredi and Andrea Dorigato. "Recycling of bioplastic waste: A review." In: *Advanced Industrial and Engineering Polymer Research* 4.3 (July 1, 2021), pp. 159–177. DOI: 10.1016/j.aiepr.2021.06.006.

[43] Edward Kosior, Jonathan Mitchell, and Irene Crescenzi. "Plastics Recycling." In: *Plastics and the Environment*. The Royal Society of Chemistry, 2019, pp. 156–176. ISBN: 978-1-78801-241-6.

[44] International Organization for Standardization. *ISO/TR 21960:2020 - Plastics*. 2020.

[45] Julien Gigault, Alexandra ter Halle, Magalie Baudrimont, Pierre-Yves Pascal, Fabienne Gauffre, Thuy-Linh Phi, Hind El Hadri, Bruno Grassl, and Stéphanie Reynaud. "Current opinion: What is a nanoplastic?" In: *Environmental Pollution* 235 (Apr. 1, 2018), pp. 1030–1034. DOI: 10.1016/j.envpol.2018.01.024.

[46] Nanna B. Hartmann et al. "Are We Speaking the Same Language? Recommendations for a Definition and Categorization Framework for Plastic Debris." In: *Environ. Sci. Technol.* 53.3 (Feb. 5, 2019), pp. 1039–1047. DOI: 10.1021/acs.est.8b05297.

[47] Delphine Kawecki and Bernd Nowack. "Polymer-Specific Modeling of the Environmental Emissions of Seven Commodity Plastics As Macro- and Microplastics." In: *Environ. Sci. Technol.* 53.16 (Aug. 20, 2019), pp. 9664–9676. DOI: 10.1021/acs.est.9b02900.

[48] Denise M. Mitrano and Wendel Wohlleben. "Microplastic regulation should be more precise to incentivize both innovation and environmental safety." In: *Nature Communications* 11.1 (Oct. 21, 2020), p. 5324. DOI: 10.1038/s41467-020-19069-1.

[49] Prangya Ranjan Rout, Anee Mohanty, Aastha, Ana Sharma, Mehak Miglani, Dezhao Liu, and Sunita Varjani. "Micro- and nanoplastics removal mechanisms in wastewater treatment plants: A review." In: *Journal of Hazardous Materials Advances* 6 (May 1, 2022), p. 100070. DOI: 10.1016/j.hazadv.2022.100070.

[50] Patricia L. Corcoran. "Degradation of Microplastics in the Environment." In: *Handbook of Microplastics in the Environment*. Ed. by Teresa Rocha-Santos, Monica F. Costa, and Catherine Mouneyrac. Cham: Springer International Publishing, 2022, pp. 531–542. ISBN: 978-3-030-39041-9.

[51] Patricia L. Corcoran, Mark C. Biesinger, and Meriem Grifi. "Plastics and beaches: A degrading relationship." In: *Marine Pollution Bulletin* 58.1 (Jan. 1, 2009), pp. 80–84. DOI: 10.1016/j.marpolbul.2008.08.022.

[52] Berit Gewert, Merle M. Plassmann, and Matthew MacLeod. "Pathways for degradation of plastic polymers floating in the marine environment." In: *Environ. Sci.: Processes Impacts* 17.9 (2015), pp. 1513–1521. ISSN: 2050-7887. DOI: 10.1039/C5EM00207A.

[53] Ali Chamas, Hyunjin Moon, Jiajia Zheng, Yang Qiu, Tarnuma Tabassum, Jun Hee Jang, Mahdi Abu-Omar, Susannah L. Scott, and Sangwon Suh. "Degradation Rates of Plastics in the Environment." In: *ACS Sustainable Chem. Eng.* 8.9 (Mar. 9, 2020), pp. 3494–3511. DOI: 10.1021/acssuschemeng.9b06635.

[54] Christoph D. Rummel, Annika Jahnke, Elena Gorokhova, Dana Kühnel, and Mechthild Schmitt-Jansen. "Impacts of Biofilm Formation on the Fate and Potential Effects of Microplastic in the Aquatic Environment." In: *Environ. Sci. Technol. Lett.* 4.7 (July 11, 2017), pp. 258–267. DOI: 10.1021/acs.estlett.7b00164.

[55] Geetika Bhagwat, Wayne O'Connor, Ian Grainge, and Thava Palanisami. "Understanding the Fundamental Basis for Biofilm Formation on Plastic Surfaces: Role of Conditioning Films." In: *Frontiers in Microbiology* 12 (2021). DOI: 10.3389/fmicb.2021.687118.

[56] Christoph D. Rummel, Oliver J. Lechtenfeld, René Kallies, Annegret Benke, Peter Herzsprung, Robby Rynek, Stephan Wagner, Annegret Potthoff, Annika Jahnke, and Mechthild Schmitt-Jansen. "Conditioning Film and Early Biofilm Succession on Plastic Surfaces." In: *Environ. Sci. Technol.* 55.16 (Aug. 17, 2021), pp. 11006–11018. DOI: 10.1021/acs.est.0c07875.

[57] Alka Kumari and Doongar R. Chaudhary. "21 - Engineered microbes and evolving plastic bioremediation technology." In: *Bioremediation of Pollutants*. Ed. by Vimal Chandra Pandey and Vijai Singh. Elsevier, Jan. 1, 2020, pp. 417–443. ISBN: 978-0-12-819025-8.

[58] Yu Yang, Jun Yang, Wei-Min Wu, Jiao Zhao, Yiling Song, Longcheng Gao, Ruifu Yang, and Lei Jiang. "Biodegradation and Mineralization of Polystyrene by Plastic-Eating Mealworms: Part 1. Chemical and Physical Characterization and Isotopic Tests." In: *Environ. Sci. Technol.* 49.20 (Oct. 20, 2015), pp. 12080–12086. DOI: 10.1021/acs.est.5b02661.

[59] Atefeh Esmaeili, Ahmad Ali Pourbabaee, Hossein Ali Alikhani, Farzin Shabani, and Ensieh Esmaeili. "Biodegradation of Low-Density Polyethylene (LDPE) by Mixed Culture of Lysinibacillus xylanilyticus and Aspergillus niger in Soil." In: *PLOS ONE* 8.9 (Sept. 23, 2013), e71720. DOI: 10.1371/journal.pone.0071720.

[60] A. Sivan, M. Szanto, and V. Pavlov. "Biofilm development of the polyethylene-degrading bacterium Rhodococcus ruber." In: *Applied Microbiology and Biotechnology* 72.2 (Sept. 1, 2006), pp. 346–352. DOI: 10.1007/s00253-005-0259-4.

[61] I. Gilan (Orr), Y. Hadar, and A. Sivan. "Colonization, biofilm formation and biodegradation of polyethylene by a strain of Rhodococcus ruber." In: *Applied Microbiology and Biotechnology* 65.1 (July 1, 2004), pp. 97–104. DOI: 10.1007/s00253-004-1584-8.

[62] Barbara J. Frisken. "Revisiting the method of cumulants for the analysis of dynamic light-scattering data." In: *Appl. Opt.* 40.24 (Aug. 20, 2001), p. 4087. DOI: 10.1364/AO.40.004087.

[63] Stephen W. Provencher. "CONTIN: A general purpose constrained regularization program for inverting noisy linear algebraic and integral equations." In: *Computer Physics Commu-*

*nications* 27.3 (Sept. 1, 1982), pp. 229–242. DOI: 10.1016/0010-4655(82)90174-6.

[64] Jake Austin, Caterina Minelli, Douglas Hamilton, Magdalena Wywijas, and Hanna Jankevics Jones. "Nanoparticle number concentration measurements by multi-angle dynamic light scattering." In: *Journal of Nanoparticle Research* 22.5 (May 6, 2020), p. 108. DOI: 10.1007/s11051-020-04840-8.

[65] Sourav Bhattacharjee. "DLS and zeta potential – What they are and what they are not?" In: *Journal of Controlled Release* 235 (Aug. 10, 2016), pp. 337–351. DOI: 10.1016/j.jconrel.2016.06.017.

[66] Alexandra Ter Halle, Laurent Jeanneau, Marion Martignac, Emilie Jardé, Boris Pedrono, Laurent Brach, and Julien Gigault. "Nanoplastic in the North Atlantic Subtropical Gyre." In: *Environ. Sci. Technol.* 51.23 (Dec. 5, 2017), pp. 13689–13697. DOI: 10.1021/acs.est.7b03667.

[67] Julia N. Möller, Martin G. J. Löder, and Christian Laforsch. "Finding Microplastics in Soils: A Review of Analytical Methods." In: *Environ. Sci. Technol.* 54.4 (Feb. 18, 2020), pp. 2078–2090. DOI: 10.1021/acs.est.9b04618.

[68] Yujian Lai, Lijie Dong, Qingcun Li, Peng Li, and Jingfu Liu. "Sampling of micro- and nano-plastics in environmental matrixes." In: *TrAC Trends in Analytical Chemistry* 145 (Dec. 1, 2021), p. 116461. DOI: 10.1016/j.trac.2021.116461.

[69] Julie Masura, Joel Baker, Gregory Foster, and Courtney Arthur. *Laboratory methods for the analysis of microplastics in the marine environment: recommendations for quantifying synthetic particles in waters and sediments*. 2015.

[70] Ana I. Catarino, Richard Thompson, William Sanderson, and Theodore B. Henry. "Development and optimization of a standard method for extraction of microplastics in mussels by enzyme digestion of soft tissues." In: *Environmental Toxicology and Chemistry* 36.4 (Apr. 1, 2017), pp. 947–951. DOI: 10.1002/etc.3608.

[71] Martin G. J. Löder and Gunnar Gerdts. "Methodology Used for the Detection and Identification of Microplastics—A Critical Appraisal." In: *Marine Anthropogenic Litter*. Ed. by Melanie Bergmann, Lars Gutow, and Michael Klages. Cham: Springer International Publishing, 2015, pp. 201–227. ISBN: 978-3-319-16510-3.

[72] Ludovic Hermabessiere et al. "Optimization, performance, and application of a pyrolysis-GC/MS method for the identification of microplastics." In: *Analytical and Bioanalytical Chemistry*

410.25 (Oct. 1, 2018), pp. 6663–6676. DOI: 10.1007/s00216-018-1279-0.

[73] Erik Hendrickson, Elizabeth C. Minor, and Kathryn Schreiner. "Microplastic Abundance and Composition in Western Lake Superior As Determined via Microscopy, Pyr-GC/MS, and FTIR." In: *Environ. Sci. Technol.* 52.4 (Feb. 20, 2018), pp. 1787–1796. DOI: 10.1021/acs.est.7b05829.

[74] E. Duemichen, P. Eisentraut, M. Celina, and U. Braun. "Automated thermal extraction-desorption gas chromatography mass spectrometry: A multifunctional tool for comprehensive characterization of polymers and their degradation products." In: *Journal of Chromatography A* 1592 (May 10, 2019), pp. 133–142. DOI: 10.1016/j.chroma.2019.01.033.

[75] Paul Eisentraut, Erik Dümichen, Aki Sebastian Ruhl, Martin Jekel, Mirko Albrecht, Michael Gehde, and Ulrike Braun. "Two Birds with One Stone—Fast and Simultaneous Analysis of Microplastics: Microparticles Derived from Thermoplastics and Tire Wear." In: *Environ. Sci. Technol. Lett.* 5.10 (Oct. 9, 2018), pp. 608–613. DOI: 10.1021/acs.estlett.8b00446.

[76] Ulrike Braun, Paul Eisentraut, Korinna Altmann, Maria Kittner, Erik Dümichen, Kurt Thaxton, Eike Kleine-Benne, and Tarun Anumol. *Accelerated Determination of Microplastics in Environmental Samples Using Thermal Extraction Desorption-Gas Chromatography/Mass Spectrometry (TED-GC/MS)*. Nov. 5, 2020. URL: https://www.agilent.com/cs/library/applications/application-microplastics-determination-by-ted-gc-msd-5994-2551en-agilent.pdf.

[77] Mikael T. Ekvall, Isabella Gimskog, Jing Hua, Egle Kelpsiene, Martin Lundqvist, and Tommy Cedervall. "Size fractionation of high-density polyethylene breakdown nanoplastics reveals different toxic response in Daphnia magna." In: *Scientific Reports* 12.1 (Feb. 24, 2022), p. 3109. DOI: 10.1038/s41598-022-06991-1.

[78] Kosuke Tanaka, Yusuke Takahashi, Hidetoshi Kuramochi, Masahiro Osako, Shunsuke Tanaka, and Go Suzuki. "Preparation of Nanoscale Particles of Five Major Polymers as Potential Standards for the Study of Nanoplastics." In: *Small* n/a (n/a Nov. 1, 2021), p. 2105781. DOI: 10.1002/smll.202105781.

[79] Mikael T. Ekvall, Martin Lundqvist, Egle Kelpsiene, Eimantas Šileikis, Stefán B. Gunnarsson, and Tommy Cedervall. "Nanoplastics formed during the mechanical breakdown of daily-use polystyrene products." In: *Nanoscale Adv.* 1.3 (2019), pp. 1055–1061. DOI: 10.1039/C8NA00210J.

[80] IKA-Werke GmbH \& CO. KG. *S 18 N - 19 G Dispersing tool - Data Sheet*. URL: https://www.ika.com/en/Products-Lab-Eq/Dispersers-Homogenizer-csp-177/S-18-N-19-G-Dispersing-tool-Downloads-cpdl-L004640/.

[81] Claudia Jacobs and Rainer Helmut Müller. "Production and Characterization of a Budesonide Nanosuspension for Pulmonary Administration." In: *Pharmaceutical Research* 19.2 (Feb. 1, 2002), pp. 189–194. DOI: 10.1023/A:1014276917363.

[82] Patrice Creux, Jean Lachaise, Alain Graciaa, James K. Beattie, and Alex M. Djerdjev. "Strong Specific Hydroxide Ion Binding at the Pristine Oil/Water and Air/Water Interfaces." In: *J. Phys. Chem. B* 113.43 (Oct. 29, 2009), pp. 14146–14150. DOI: 10.1021/jp906978v.

[83] Ralf Zimmermann, Uwe Freudenberg, Rüdiger Schweiß, David Küttner, and Carsten Werner. "Hydroxide and hydronium ion adsorption — A survey." In: *Current Opinion in Colloid & Interface Science* 15.3 (June 1, 2010), pp. 196–202. DOI: 10.1016/j.cocis.2010.01.002.

[84] Ralf Zimmermann, Nelly Rein, and Carsten Werner. "Water ion adsorption dominates charging at nonpolar polymer surfaces in multivalent electrolytes." In: *Phys. Chem. Chem. Phys.* 11.21 (2009), pp. 4360–4364. DOI: 10.1039/B900755E.

[85] Jana Hildebrandt and Andreas F. Thünemann. "Aqueous Dispersions of Polypropylene: Toward Reference Materials for Characterizing Nanoplastics." In: *Macromolecular Rapid Communications* 44.6 (Mar. 1, 2023), p. 2200874. DOI: 10.1002/marc.202200874.

[86] International Organization for Standardization. *ISO Guide 35:2017(E) Reference materials - Guidance for characterization and assessment of homogeneity and stability*. 2017.

[87] Denise M. Mitrano, Anna Beltzung, Stefan Frehland, Michael Schmiedgruber, Alberto Cingolani, and Felix Schmidt. "Synthesis of metal-doped nanoplastics and their utility to investigate fate and behaviour in complex environmental systems." In: *Nature Nanotechnology* 14.4 (Apr. 1, 2019), pp. 362–368. DOI: 10.1038/s41565-018-0360-3.

[88] Gordana Bogoeva-Gaceva, Aco Janevski, and Anita Grozdanov. "Crystallization and melting behavior of iPP studied by DSC." In: *Journal of Applied Polymer Science* 67.3 (Jan. 18, 1998), pp. 395–404. DOI: 10.1002/(SICI)1097-4628(19980118)67:3<395::AID-APP2>3.0.CO;2-H.

[89] Ján Malík and Christoph Kröhnke. "Polymer stabilization: present status and possible future trends." In: *Comptes Rendus Chimie* 9.11 (Nov. 1, 2006), pp. 1330–1337. DOI: 10.1016/j.crci.2006.02.009.

[90] C. Kröhnke and F. Werner. *Stabilisers for Polyolefins - Rapra Review Reports: Experts overviews covering the science and technology of rubber and plastics*. Vol. 11. Rapra Review Reports 12. Rapra Technology Ltd., 2001. ISBN: 978-1-85957-285-6.

[91] Lars Kool, Anton Bunschoten, Aldrik H. Velders, and Vittorio Saggiomo. "Gold nanoparticles embedded in a polymer as a 3D-printable dichroic nanocomposite material." In: *Beilstein J. Nanotechnol.* 10 (2019), pp. 442–447. DOI: 10.3762/bjnano.10.43.

[92] Zhitian Ding, Ruiying Bao, Bo Zhao, Jing Yan, Zhengying Liu, and Mingbo Yang. "Effects of annealing on structure and deformation mechanism of isotactic polypropylene film with row-nucleated lamellar structure." In: *Journal of Applied Polymer Science* 130.3 (Nov. 5, 2013), pp. 1659–1666. DOI: 10.1002/app.39351.

[93] N. Morosoff, K. Sakaoku, and A. Peterlin. "Crystallite size in drawn and then annealed polypropylene." In: *Journal of Polymer Science Part A-2: Polymer Physics* 10.7 (July 1, 1972), pp. 1221–1236. ISSN: 0449-2978. DOI: 10.1002/pol.1972.160100704.

[94] Glen J. Smales and Brian R. Pauw. "The MOUSE project: a meticulous approach for obtaining traceable, wide-range X-ray scattering information." In: *Journal of Instrumentation* 16.6 (June 24, 2021), P06034. DOI: 10.1088/1748-0221/16/06/P06034.

[95] A. L. Patterson. "The Scherrer Formula for X-Ray Particle Size Determination." In: *Phys. Rev.* 56.10 (Nov. 15, 1939), pp. 978–982. DOI: 10.1103/PhysRev.56.978.

[96] P. W. Bridgman. "Certain Physical Properties of Single Crystals of Tungsten, Antimony, Bismuth, Tellurium, Cadmium, Zinc, and Tin." In: *Proceedings of the American Academy of Arts and Sciences* 60.6 (1925), pp. 305–383. DOI: 10.2307/25130058.

[97] J. Czochralski. "Ein neues Verfahren zur Messung der Kristallisationsgeschwindigkeit der Metalle." In: Zeitschrift für Physikalische Chemie 92U.1 (1918), pp. 219–221. DOI: 10.1515/zpch-1918-9212.

[98] C. Coutinho, E. Bernardes, Durvalina Félix, and Anita D. Panek. "Trehalose as cryoprotectant for preservation of yeast strains." In: *Journal of Biotechnology* 7.1 (Jan. 1, 1988), pp. 23–32. DOI: 10.1016/0168-1656(88)90032-6.

[99] Iqbal S. Bhandal, Randal M. Hauptmann, and Jack M. Widholm. "Trehalose as Cryoprotectant for the Freeze Preservation of Carrot and Tobacco Cells 1." In: *Plant Physiology* 78.2 (June 1, 1985), pp. 430–432. DOI: 10.1104/pp.78.2.430.

[100] Ingo Breßler. *Particle concentration from DLS data*. BAMresearch. Feb. 20, 2023. URL: https://github.com/BAMresearch/particle_concentration_from_dls.

[101] Yizhong Lu and Wei Chen. "Sub-nanometre sized metal clusters: from synthetic challenges to the unique property discoveries." In: *Chem. Soc. Rev.* 41.9 (2012), pp. 3594–3623. DOI: 10.1039/C2CS15325D.

[102] Michael Walter, Jaakko Akola, Olga Lopez-Acevedo, Pablo D. Jadzinsky, Guillermo Calero, Christopher J. Ackerson, Robert L. Whetten, Henrik Grönbeck, and Hannu Häkkinen. "A unified view of ligand-protected gold clusters as superatom complexes." In: *Proceedings of the National Academy of Sciences* 105.27 (July 8, 2008), pp. 9157–9162. DOI: 10.1073/pnas.0801001105. (Visited on 06/26/2023).

[103] Wen Wu Xu, Xiao Cheng Zeng, and Yi Gao. "Application of Electronic Counting Rules for Ligand-Protected Gold Nanoclusters." In: *Acc. Chem. Res.* 51.11 (Nov. 20, 2018), pp. 2739–2747. DOI: 10.1021/acs.accounts.8b00324.

[104] Rongchao Jin. "Atomically precise metal nanoclusters: stable sizes and optical properties." In: *Nanoscale* 7.5 (2015), pp. 1549–1565. DOI: 10.1039/C4NR05794E.

[105] Jing Chen, Qian-Fan Zhang, Timary A. Bonaccorso, Paul G. Williard, and Lai-Sheng Wang. "Controlling Gold Nanoclusters by Diphospine Ligands." In: *J. Am. Chem. Soc.* 136.1 (Jan. 8, 2014), pp. 92–95. DOI: 10.1021/ja411061e.

[106] Xun Yuan, Bin Zhang, Zhentao Luo, Qiaofeng Yao, David Tai Leong, Ning Yan, and Jianping Xie. "Balancing the Rate of Cluster Growth and Etching for Gram-Scale Synthesis of Thiolate-Protected Au25 Nanoclusters with Atomic Precision." In: *Angewandte Chemie International Edition* 53.18 (Apr. 25, 2014). Publisher: John Wiley & Sons, Ltd, pp. 4623–4627. DOI: 10.1002/anie.201311177. (Visited on 06/26/2023).

[107] Christoph Janiak. "Metal Nanoparticle Synthesis in Ionic Liquids." In: *Ionic Liquids (ILs) in Organometallic Catalysis*. Ed. by Jairton Dupont and László Kollár. Berlin, Heidelberg: Springer Berlin Heidelberg, 2015, pp. 17–53. ISBN: 978-3-662-47857-8. DOI: 10.1007/3418_2013_70.

[108] Sylvie Rangan, Jonathan Viereck, and Robert A. Bartynski. "Electronic Properties of Cyano Ionic Liquids: a Valence Band Photoemission Study." In: *J. Phys. Chem. B* 124.36 (Sept. 10, 2020), pp. 7909–7917. DOI: 10.1021/acs.jpcb.0c06423.

[109] Florian Fetzer, Nia Pollard, Nadine C. Michenfelder, Markus Strienz, Andreas N. Unterreiner, Andre Z. Clayborne, and Andreas Schnepf. "Au20(tBu3P)8: A Highly Symmetric Metalloid Gold Cluster in Oxidation State 0." In: *Angewandte Chemie International Edition* 61.36 (Sept. 5, 2022), e202206019. DOI: 10.1002/anie.202206019.

[110] Jörg Polte, T. Torsten Ahner, Friedmar Delissen, Sergey Sokolov, Franziska Emmerling, Andreas F. Thünemann, and Ralph Kraehnert. "Mechanism of Gold Nanoparticle Formation in the Classical Citrate Synthesis Method Derived from Coupled In Situ XANES and SAXS Evaluation." In: *J. Am. Chem. Soc.* 132.4 (Feb. 3, 2010), pp. 1296–1301. DOI: 10.1021/ja906506j.

[111] Manzhou Zhu, Christine M. Aikens, Frederick J. Hollander, George C. Schatz, and Rongchao Jin. "Correlating the Crystal Structure of A Thiol-Protected Au25 Cluster and Optical Properties." In: *J. Am. Chem. Soc.* 130.18 (May 1, 2008), pp. 5883–5885. DOI: 10.1021/ja801173r.

[112] Ingo Breßler, Joachim Kohlbrecher, and Andreas F. Thünemann. "SASfit: a tool for small-angle scattering data analysis using a library of analytical expressions." In: *Journal of Applied Crystallography* 48.5 (Oct. 2015), pp. 1587–1598. DOI: 10.1107/S1600576715016544.

[113] Risako Tsunoyama, Hironori Tsunoyama, Panvika Pannopard, Jumras Limtrakul, and Tatsuya Tsukuda. "MALDI Mass Analysis of 11 kDa Gold Clusters Protected by Octadecanethiolate Ligands." In: *J. Phys. Chem. C* 114.38 (Sept. 30, 2010), pp. 16004–16009. DOI: 10.1021/jp101741a.

[114] Jana Hildebrandt, Andreas Taubert, and Andreas F. Thünemann. "Synthesis and Characterization of Ultra-Small Gold Nanoparticles in the Ionic Liquid 1-Ethyl-3-methylimidazolium Dicyanamide, [Emim][DCA]." In: *ChemistryOpen* (Aug. 31, 2023). Publisher: John Wiley & Sons, Ltd, e202300106. DOI: 10.1002/open.202300106.

[115] Cui-Wei Wang, Shi-Ping Yang, He Hu, Jing Du, and Feng-Hua Li. "Synthesis, characterization and in vitro and in vivo investigation of C3F8-filled poly(lactic-co-glycolic acid) nanoparticles as an ultrasound contrast agent." In: *Mol Med Rep* 11.3 (Mar. 1, 2015), pp. 1885–1890. DOI: 10.3892/mmr.2014.2938.

[116] J. Filik et al. "Processing two-dimensional X-ray diffraction and small-angle scattering data in DAWN 2." In: *Journal of Applied Crystallography* 50.3 (June 2017), pp. 959–966. DOI: 10.1107/S1600576717004708.

[117] B. R. Pauw, A. J. Smith, T. Snow, N. J. Terrill, and A. F. Thünemann. "The modular small-angle X-ray scattering data correction sequence." In: *Journal of Applied Crystallography* 50.6 (Dec. 2017), pp. 1800–1811. DOI: 10.1107/S1600576717015096.

[118] Ingo Breßler, Brian Pauw, and Andreas Thünemann. "McSAS: Software for the retrieval of model parameter distributions from scattering patterns." In: *Journal of Applied Crystallography* 48 (June 1, 2015). DOI: 10.1107/S1600576715007347.

[119] J Spreadborough and J W Christian. "High-temperature X-ray diffractometer." In: *Journal of Scientific Instruments* 36.3 (Mar. 1, 1959), p. 116. DOI: 10.1088/0950-7671/36/3/302.

[120] Gunasekaran Suriyakala, Sivaji Sathiyaraj, Ranganathan Babujanarthanam, Khaloud Mohammed Alarjani, Dina S. Hussein, Rabab Ahmed Rasheed, and K. Kanimozhi. "Green synthesis of gold nanoparticles using Jatropha integerrima Jacq. flower extract and their antibacterial activity." In: *Journal of King Saud University - Science* 34.3 (Apr. 1, 2022), p. 101830. DOI: 10.1016/j.jksus.2022.101830.

# A

# APPENDIX

## A.1 FURTHER INFORMATION

*ANOVA tables*

One-way ANOVA tests were performed for the homogeneity studies of the polyolefin reference material candidates for each measurand, i. e. $D_h$, PDI and $\zeta$ potential. The null hypothesis in these cases was, that the datasets from day 1, day 2 and day 3 have the same mean. The confidence level was set to 0.95 resulting in a maximum 5% probability of false rejection of the null hypothesis. The critical $F$-value $F_{crit}$ was calculated with the degrees of freedom to be 1.853 for each measurand. The null hypothesis is rejected if the F value calculated is bigger than the critical F value.

*nanoPP*

Detailed overview of the results of the ANOVA tests for the homogeneity study of the nanoPP reference material candidate. The samples were filtered before measurement.

Table A.1: ANOVA results for between-bottle homogeneity study of $D$

| Overall Mean (nm) | Overall $s$ (nm) | Source of variation | $SS$ | $df$ | $MS$ | $s$ | F | $F_{crit}$ | $p$-value |
|---|---|---|---|---|---|---|---|---|---|
| 180.5 | 5.76 | Between bottles | 893.39 | 19 | 47.021 | 2.613 | 1.772 | 1.853 | 0.064 |
| | | Within bottles | 1061.7 | 40 | 26.542 | 5.152 | | | |
| | | Total | 1955.1 | 59 | | | | | |

Table A.2: ANOVA results for between-bottle homogeneity study of PDI

| Overall Mean | Overall $s$ | Source of variation | $SS$ | $df$ | $MS$ | $s$ | F | $F_{crit}$ | $p$-value |
|---|---|---|---|---|---|---|---|---|---|
| 0.084 | 0.023 | Between bottles | 0.011 | 19 | 0.001 | 0.004 | 1.102 | 1.853 | 0.385 |
| | | Within bottles | 0.021 | 40 | 0.001 | 0.023 | | | |
| | | Total | 0.032 | 59 | | | | | |

Table A.3: ANOVA results for between-bottle homogeneity study of $\zeta$ potential

| Overall Mean (mV) | Overall $s$ (mV) | Source of variation | $SS$ | $df$ | $MS$ | $s$ | F | $F_{crit}$ | $p$-value |
|---|---|---|---|---|---|---|---|---|---|
| -42.998 | 1.97 | Between bottles | 65.07 | 19 | 3.425 | 0.0 | 0.835 | 1.853 | 0.656 |
| | | Within bottles | 164.1 | 40 | 4.102 | 2.025 | | | |
| | | Total | 229.17 | 59 | | | | | |

*nanoPE*

Detailed overview of the results of the ANOVA tests for the homogeneity study of the nanoPE reference material candidate. The samples were filtered before measurement.

Table A.4: ANOVA results for between-bottle homogeneity study of $D$

| Overall Mean (nm) | Overall $s$ (nm) | Source of variation | $SS$ | $df$ | $MS$ | $s$ | F | $F_{crit}$ | $p$-value |
|---|---|---|---|---|---|---|---|---|---|
| 164.48 | 19.3 | Between bottles | 3996.5 | 19 | 210.34 | 0.0 | 0.466 | 1.853 | 0.962 |
| | | Within bottles | 18050.0 | 40 | 451.25 | 21.24 | | | |
| | | Total | 22046.0 | 59 | | | | | |

Table A.5: ANOVA results for between-bottle homogeneity study of PDI

| Overall Mean | Overall $s$ | Source of variation | $SS$ | $df$ | $MS$ | $s$ | F | $F_{crit}$ | $p$-value |
|---|---|---|---|---|---|---|---|---|---|
| 0.188 | 0.061 | Between bottles | 0.035 | 19 | 0.002 | 0.0 | 0.404 | 1.853 | 0.982 |
| | | Within bottles | 0.185 | 40 | 0.005 | 0.068 | | | |
| | | Total | 0.22 | 59 | | | | | |

Table A.6: ANOVA results for between-bottle homogeneity study of $\zeta$-potential

| Overall Mean (mV) | Overall $s$ (mV) | Source of variation | $SS$ | $df$ | $MS$ | $s$ | F | $F_{crit}$ | $p$-value |
|---|---|---|---|---|---|---|---|---|---|
| -37.912 | 1.98 | Between bottles | 152.04 | 19 | 8.002 | 1.419 | 4.08 | 1.853 | 0.0 |
| | | Within bottles | 78.46 | 40 | 1.962 | 1.401 | | | |
| | | Total | 230.5 | 59 | | | | | |

The homogeneity and ANOVA study were also performed for samples not filtered before measurement.

Table A.7: ANOVA results for between-bottle homogeneity study of $D$

| Overall Mean (nm) | Overall $s$ (nm) | Source of variation | $SS$ | $df$ | $MS$ | $s$ | F | $F_{crit}$ | $p$-value |
|---|---|---|---|---|---|---|---|---|---|
| 344.52 | 34.6 | Between bottles | 21212.0 | 19 | 1116.4 | 0.0 | 0.902 | 1.853 | 0.584 |
| | | Within bottles | 49536.0 | 40 | 1238.4 | 35.19 | | | |
| | | Total | 70749.0 | 59 | | | | | |

Table A.8: ANOVA results for between-bottle homogeneity study of PDI

| Overall Mean | Overall $s$ | Source of variation | $SS$ | $df$ | $MS$ | $s$ | F | $F_{crit}$ | $p$-value |
|---|---|---|---|---|---|---|---|---|---|
| 0.388 | 0.042 | Between bottles | 0.032 | 19 | 0.002 | 0.0 | 0.937 | 1.853 | 0.546 |
| | | Within bottles | 0.072 | 40 | 0.002 | 0.042 | | | |
| | | Total | 0.104 | 59 | | | | | |

Table A.9: ANOVA results for between-bottle homogeneity study of $\zeta$-potential

| Overall Mean (mV) | Overall $s$ (mV) | Source of variation | $SS$ | $df$ | $MS$ | $s$ | F | $F_{crit}$ | $p$-value |
|---|---|---|---|---|---|---|---|---|---|
| -40.003 | 4.21 | Between bottles | 330.97 | 19 | 17.419 | 0.0 | 0.974 | 1.853 | 0.508 |
| | | Within bottles | 715.29 | 40 | 17.882 | 4.229 | | | |
| | | Total | 1046.3 | 59 | | | | | |

*Crystallographic calculations of gold in PP matrix*

The BRAGG equation

$$n\lambda = 2d \sin\theta$$

is used to determine the crystalline properties of structures. It is dependent on the half scattering angle $\theta$. Therefore, the obtained scattering data which depend on the scattering vector $q$ have to be converted to $2\theta$-dependent data.
The reflection of interest occurs at $q = 26.46\ \mathrm{nm}^{-1}$, which equals $2\theta = 37.84°$ using the relation given in Equation 2.2 for Cu $K_\alpha$ radiation with $\lambda = 0.154$ nm. Comparing the database data of Au (obtained from Crystallographic Open Database entry 1100138 based on the data from [119]), the reflection at $2\theta = 38.27°$ is the one closest.

Table A.10: Table of reflection parameters for Au in the range of $2\theta = 35° - 45°$ calculated with data from [119].

| No. | $2\theta$ (°) | $d$ (nm) | $h$ | $k$ | $l$ |
|---|---|---|---|---|---|
| 1 | 38.272 | 0.23498 | 1 | 1 | 1 |
| 2 | 44.485 | 0.20350 | 0 | 0 | 2 |

The slight deviation is due to the measurement uncertainty of the instrument and the sample. Therefore, the reflection at $2\theta = 38.27°$ equals the reflection of the Au(111) plane.

The peak of the Au(111) plane in the SAXS data, can also be analysed to determine the size of the crystallites present in the gold structures found in the PP. For a single reflection, the SCHERRER equation [95] is used.

$$D_{hkl} = \frac{k\lambda}{B_{\mathrm{sample}} \cos\theta}$$

For gold, the shape factor $k$ is 0.9 [120]. $B_{\mathrm{sample}}$ is the FWHM of the Gaussian fit of the peak, which is 0.46°. This has to be reduced by the broadening based on the instrument, which is 0.31° [24]. Finally, is $B_{\mathrm{sample}} = 0.15°$. The $\theta$ of the peak maximum is 18.92°. The result is $D_{hkl} = 0.98$ nm. The Gaussian fit of the Au(111) peak is shown in Figure A.1.

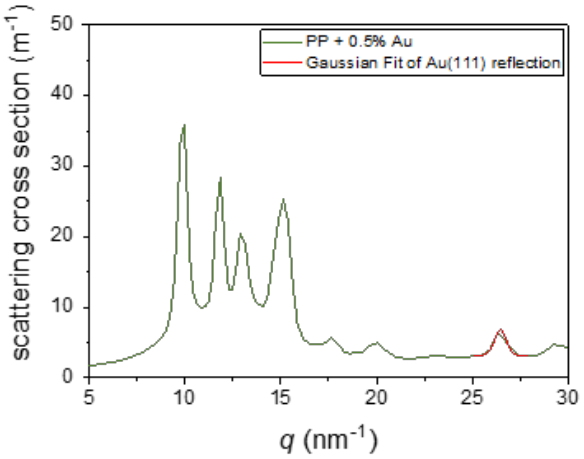


Figure A.1: SAXS data

## A.2 PUBLICATIONS

*Publications featured in this thesis*

- Jana Hildebrandt and Andreas F. Thünemann. "Aqueous Dispersions of Polypropylene: Toward Reference Materials for Characterizing Nanoplastics." In: *Macromolecular Rapid Communications* 44.6 (Mar. 1, 2023), p. 2200874. DOI: 10.1002/marc.202200874.
- Jana Hildebrandt, Andreas Taubert, and Andreas Thünemann. "Synthesis and Characterization of Ultra-Small Gold Nanoparticles in the Ionic Liquid 1-Ethyl-3-methylimidazolium Dicyanamide, [Emim][DCA]." In: *ChemistryOpen* (Aug. 31, 2023). DOI: 10.1002/open.202300106.

*Publications not featured in this thesis*

Malín G. Lüdicke, Jana Hildebrandt, Christoph Schindler, Ralph A. Sperling, and Michael Maskos. "Automated Quantum Dots Purification via Solid Phase Extraction." In: *Nanomaterials* 12.12 (2022). DOI: 10.3390/nano12121983.

## A.3 CONFERENCE CONTRIBUTIONS

*Presentations*

- Jana Hildebrandt and Andreas Thünemann. "PP and PE nanoplastics in water." *48$^{th}$ World Polymer Congress - IUPAC - MACRO2020+*, Jeju, South Korea, hybrid conference, 2021.
- Jana Hildebrandt and Andreas Thünemann. "Aqueous Dispersions of polypropylene as possible reference material for nanoplastics." *European Polymer Congress*, Prague, Czech Republic, 2022.

*Posters*

- Jana Hildebrandt and Andreas Thünemann. "Polypropylene and polyethylene nanoplastics in water." *Tag der Chemie 2021*, University of Potsdam, online, 2021.
- Jana Hildebrandt and Andreas Thünemann. "Preparation of polypropylene and polyethylene nanoplastics in water." *101 years of Macromolecular Chemistry*, online, 2021.
- Jana Hildebrandt and Andreas Thünemann. "PP Nanoplastics Dispersed in Water As Reference Materials." *Prague Meeting on Macromolecules 2022*, Prague, Czech Republic, 2022.

- Jana Hildebrandt and Andreas Thünemann. "Aqueous dispersions of polypropylene: towards reference materials for nanoplastics characterization." *International Conference on Microplastic Pollution in the Mediterranean Sea*, Naples, Italy, 2022.

# DECLARATION

I hereby confirm: The submitted work was carried out independently and only explicitly listed sources and means were used.
Furthermore, I confirm that this thesis has not been submitted elsewhere for the purpose of obtaining a doctoral degree.

Hiermit versichere ich: Die vorliegende Arbeit wurde selbstständig durchgeführt. Es wurden keine anderen Quellen und Hilfsmittel als die ausdrücklich aufgeführten verwendet.
Weiterhin versichere ich, dass diese Arbeit noch nicht an anderer Stelle zur Erlangung des Doktorgrades eingereicht worden ist.

*Berlin, July 2023*

Jana Hildebrandt